



PCCP

**A critical comparison of CH... $\pi$  versus  $\pi$ ... $\pi$  interactions in the benzene dimer: obtaining benchmarks at the CCSD(T) level and assessing the accuracy of lower scaling methods**

Journal:	<i>Physical Chemistry Chemical Physics</i>
Manuscript ID	CP-ART-09-2022-004335.R1
Article Type:	Paper
Date Submitted by the Author:	26-Nov-2022
Complete List of Authors:	Herman, Kristina; University of Washington Aprà, Edoardo; Pacific Northwest National Laboratory, Environmental Molecular Sciences Laboratory Xantheas, Sotiris; Pacific Northwest National Laboratory, Physical Sciences Division

SCHOLARONE™  
Manuscripts

# A critical comparison of CH $\cdots$ $\pi$ versus $\pi\cdots\pi$ interactions in the benzene dimer: obtaining benchmarks at the CCSD(T) level and assessing the accuracy of lower scaling methods

Kristina M. Herman,<sup>a</sup> Edoardo Aprà,<sup>b</sup> and Sotiris S. Xantheas<sup>a, c, \*</sup>

<sup>a</sup> Department of Chemistry, University of Washington, Seattle, WA 98195, USA

<sup>b</sup> Environmental Molecular Sciences Laboratory, Pacific Northwest National Laboratory, P.O. Box 999, Richland, Washington 99352, USA

<sup>c</sup> Advanced Computing, Mathematics and Data Division, Pacific Northwest National Laboratory, 902 Battelle Boulevard, P.O. Box 999, MS K1-83, WA, 99352, USA

## Abstract

We have established CCSD(T)/CBS (Complete Basis Set) limits for 3 stationary points on the benzene dimer potential energy surface, corresponding to the  $\pi\cdots\pi$  (parallel displaced or PD(C2h), minimum) and CH $\cdots$  $\pi$  (T-shaped or T(C2v), transition state) and Tilted T-shaped or TT(Cs), minimum) bonding scenarios considering *both* the structure and binding energy. The CCSD(T)/CBS binding energies are  $-2.65 \pm 0.02$  (PD),  $-2.74 \pm 0.03$  (T), and  $-2.83 \pm 0.01$  kcal/mol (TT). To this end, the CH $\cdots$  $\pi$  is  $\sim 0.2$  kcal/mol stronger than the  $\pi\cdots\pi$  interaction, whereas the tilting of the CH donating benzene molecule with respect to the other benzene is worth 0.1 kcal/mol. As previously discussed in the literature, the MP2 level of theory does not provide a close match for either the energy or structure, yet the SCS-MP2 yields structures in excellent agreement with respect to the CCSD(T) result. It is found that the SCS-MI-MP2 also gives optimized structures very close to SCS-MP2 (within  $\sim 0.01$  Å of the benchmark). Despite the closer match in structure, the spin-biased MP2 methods (SCS-, SCS-MI-, and SOS-MP2) *incorrectly*

---

\* Corresponding author. Email: [sotiris.xantheas@pnnl.gov](mailto:sotiris.xantheas@pnnl.gov) and [xantheas@uw.edu](mailto:xantheas@uw.edu)

predict the relative stabilities of the isomers. That said, none of the spin biased MP2 method offer a good compromise between energy and structure for the systems examined. Finally, the CCSD(T)/CBS benchmarks were used to assess the performance of 13 DFT functionals selected from different rungs of Jacob's ladder. Several functionals such as TPSS-D3, B3LYP-D3, B97-D, B97-D3, and B2PLYP-D3 provided a good description of the binding energies for both CH $\cdots$  $\pi$  and  $\pi\cdots\pi$  interactions, yielding values within 6% of the CCSD(T)/CBS benchmark values. Unlike the MP2 methods, these functionals correctly predict the relative stability of the PD( $C_{2h}$ ) and T( $C_{2v}$ ) dimers. Further, we find that there is no systematic improvement as Jacob's ladder is ascended (increased complexity of functional). The best functionals that result in a good compromise between structure and energy accuracy are B97-D3 and B2PLYP-D3 for both the CH $\cdots$  $\pi$  and  $\pi\cdots\pi$  interaction. Despite the impressive performance of these functionals, a challenge that remains is ensuring the transferability of these density functionals in accurately describing the interaction between dimers of larger aromatic molecules, the latter requiring high-level benchmarks for these systems.

## I. Introduction

The benzene dimer is the simplest system exhibiting  $\text{CH}\cdots\pi$  and  $\pi\cdots\pi$  interactions making it a tractable analog for studying aromatic intermolecular interactions in biomolecules. Both  $\text{CH}\cdots\pi$  and  $\pi\cdots\pi$  non-covalent bonding scenarios exist between aromatic amino acid residues in proteins and between nucleic acid bases in DNA, respectively. Furthermore, it has been established that a high percentage of aromatic amino acids participate in either  $\text{CH}\cdots\pi$  or  $\pi\cdots\pi$  bonds, strongly stabilizing the secondary structure of the protein.<sup>1-4</sup> For this reason, the accurate description of these different interactions in biomolecules is paramount in understanding processes such as protein folding,<sup>5</sup> protein-protein interactions,<sup>5</sup> and carbohydrate binding/recognition.<sup>6,7</sup> However, because  $\text{CH}\cdots\pi$  and  $\pi\cdots\pi$  interactions are often dominated by dispersion<sup>8,9</sup> or higher order multipolar electrostatic interactions, the computed binding energies are sensitive to the level of theory, often requiring highly correlated electronic structure methods such as Coupled Cluster Singles, Doubles, and perturbative Triple replacements [CCSD(T)] for reliable results. Given that the canonical formulation of this method scales as  $\mathcal{O}(N^7)$ , where  $N$  is the size of the system, it quickly becomes computationally infeasible for large systems. This motivates the development of lower-scaling methods and protocols that produce accurate binding energies at a lower computational cost. With these methods, *ab initio* computations of larger proteins and biological systems will become more feasible while also providing accurate descriptions of the elusive  $\text{CH}\cdots\pi$  and  $\pi\cdots\pi$  interactions.

The benzene dimer has been the focus of numerous computational studies aimed at understanding the energy landscape and also the computational methods and protocols that can be used to accurately describe it.<sup>10-25</sup> Past work has shown that there are numerous low-energy minima including the parallel displaced (PD), T-shaped, and tilted T-shape in addition to higher energy minima (i.e., sandwich structure). Many of these previous studies have relied on different computational methods such as CCSD(T),<sup>11-16,20,22,24,25</sup> MP2,<sup>11,13,14,16,20,23</sup> MP4,<sup>14,23</sup> SAPT,<sup>15</sup> QCISDT,<sup>10</sup> VMC,<sup>21</sup> DMC<sup>21</sup>, and recently CCSDT(Q).<sup>26</sup> A collection of the previously reported results at various levels of theory for the benzene dimer conformations reported in this study is given in Table S1 of the Supporting Information (SI). Depending on the computational protocol (i.e., level of theory, optimization, basis set, etc.), a wide range of binding energies have been previously reported. Even within the same level of theory, for example CCSD(T), estimated

binding energies range from 2.4-2.84 kcal/mol for the T-shaped dimer and 2.1-3.0 kcal/mol for the PD dimer.<sup>11-14,16,24,25</sup> To that end, it is unclear (within the margin of error) which conformation of the benzene dimer is the global minimum. A consistent computational protocol combined with a high level of theory is thus required for the accurate and precise estimation of the dissimilar interactions present in the benzene dimer.

While the dynamical nature of the gas phase benzene dimer is quite fluxional (flipping between the tilted T-shape and PD dimers),<sup>27</sup> accurately describing the structure and binding energies at the stationary points considered in this study is useful in assessing the performance of lower-scaling methods capable on CH $\cdots\pi$  and  $\pi\cdots\pi$  interactions. Note that in biological systems this fluxionality is quenched by the presence of additional steric interactions, which “lock” the positions of aromatic rings to geometries resembling the scenarios described in this study. Ultimately, the ability to accurately describe the energetics and structural components of minima on the benzene dimer PES is a test of their ability to accurately describe interactions dominated by dispersion and higher multipolar interactions. This work provides the required reference values that are the prerequisite of forthcoming results for the dimers of larger aromatic compounds (such as the Coronene dimer) to investigate whether DFT functionals or corrections of MP2 that best reproduce the results for various binding scenarios for the dimers of smaller aromatic ring dimer also do so for the larger ones. The results from this work, which establishes the baseline for these forthcoming studies, will aid in the understanding of the performance of lower-scaling methods for interactions that are notably more difficult to reproduce.

The MP2 level of theory has been shown to perform well on hydrogen bound systems,<sup>28</sup> but it inherently overestimates dispersion interactions. For this system, it has been known that MP2 greatly overestimates the binding energy.<sup>10,11,14,22</sup> Miliordos *et. al*, in a previous study on the  $\pi\cdots\pi$  interactions in the benzene dimer,<sup>13</sup> showed that the MP2/CBS level of theory converges to binding energy that is nearly double of the CCSD(T)/CBS value. Instead, spin-component scaled MP2 (SCS-MP2) produced a value much closer to CCSD(T). Thus, for the PD benzene dimer, SCS-MP2 yields  $N^7$  quality results at  $N^5$  cost, where  $N$  is the size of the system. In addition to MP2, density functional theory (DFT) is often a convenient method that is widely used because of its relatively low computational cost (with a formal scaling of  $N^3 - N^4$ ). The functionals are organized into rungs of “Jacob’s ladder”<sup>29,30</sup> based on their complexity, ranging from a simple local density

approximation (LDA) up to double hybrid functionals that incorporate components of exact exchange and PT2 correlation energy. However, there is no systematic way to predict the accuracy of the DFT functionals *a priori*, i.e., it is not the case that the functionals in the higher rungs of Jacobs ladder will always produce more accurate results, and the accuracy often varies based on the system of interest. Therefore, one must test the results with the various functionals against an accurate benchmark obtained using a highly correlated method to ensure their trustworthiness.<sup>31,32</sup>

The goal of this study is to build upon our earlier study<sup>13</sup> of the parallel displacement ( $\pi\cdots\pi$ ) arrangement of the benzene dimer by providing CCSD(T)/CBS binding energies for several arrangements of the T-shape ( $\text{CH}\cdots\pi$ ) configuration. This combined set of benchmark data for both the intermolecular distances and binding energies in the two arrangements is used to determine the performance of lower-scaling methods (DFT and spin biased MP2 corrections). The  $\text{CH}\cdots\pi$  conformations examined in this study include the T-shape (T) and variations of the tilted T-shape (TT) that have been reported in earlier studies.<sup>15</sup> The MP2 and CCSD(T) energies were calculated using basis sets of various sizes in order to extrapolate to the complete basis set limit. In addition, spin biased corrections to MP2 (i.e., SCS-MP2, SCS-MI-MP2, SOS-MP2) were investigated due to the impressive performance of the spin-component scaled correction (SCS-MP2) on the parallel displaced (PD) dimer system.<sup>13</sup> Lastly, DFT functionals from various rungs of Jacob's ladder were tested against the CCSD(T) results for both the PD and T-shaped conformers to identify functionals capable of accurately describing both bonding scenarios. Importantly, the Grimme D3 dispersion correction<sup>33,34</sup> (where applicable) was applied to the density functionals to provide a better description of the dispersive forces that dominate these benzene dimer interactions. The results in this paper provide valuable insight into the accuracy of lower scaling computational methods in representing biologically relevant  $\text{CH}\cdots\pi$  and  $\pi\cdots\pi$  interactions. These methods may allow for more accurate (and computationally feasible) calculations on proteins, DNA, and other biomolecules.

## II. Computational Details

**a. MP2 and spin biased MP2 calculations:** The  $T(C_{2v})$  and  $TT(C_s)$  structures were optimized under the corresponding symmetries specified in the parentheses. The two electron integrals were computed using a Schwarz screening threshold of 1.0E-15 and SCF energies were converged with

a threshold of 1.0E-9 Hartree. Given that the potential energy surface of the benzene dimer is notably flat, the “tight” convergence criterion of the geometry optimizations was specified. The family of Dunning augmented correlation consistent basis sets,<sup>35</sup> aug-cc-pVnZ  $n = 2 - 5$ , were utilized for a systematic convergence to the complete basis set (CBS) limit. Extrapolation to the CBS limit was performed by fitting the binding energies at increasing basis set sizes to the following double exponential<sup>36</sup>

$$D_e(n) = D_e(\infty) + Ae^{-(n-1)} + Be^{-(n-1)^2} \quad (1)$$

which was used earlier for the extrapolations by Miliordos *et. al* on the PD dimer.<sup>13</sup> The parameters  $A$  and  $B$  are fitted and the variable  $n$  is the size of the basis set (aug-cc-pVnZ). Note that several previous studies<sup>13,37-41</sup> have demonstrated that geometric and energetic quantities with the two families of plain (cc-pVnZ) and augmented (aug-cc-pVnZ) sets with increasing  $n$  converge to the same limit (CBS), albeit faster for the augmented family. However, the existence of diffuse functions in the family of augmented sets causes the existence of linear dependencies that are oftentimes difficult to handle. To this end, the use of the family of just the plain (cc-pVnZ) sets offers a more efficient path to reach the CBS limit. Further, as the CBS limit is approached with increasing basis set sizes, the uncorrected and BSSE-corrected binding energies will also approach the same value (since the BSSE is an artifact of an incomplete basis set). That said, the uncorrected values are also included on the extrapolation plots. The uncorrected and BSSE-corrected values are extrapolated to the CBS limit independently. The deviation between the two values is used as a measure of uncertainty in the extrapolation. In some cases, it has been shown that the average of the uncorrected and BSSE-corrected values closely matches the CBS binding energy, offering a cheaper way of approximating the CBS value from smaller basis set sizes.<sup>13,42</sup> In the interest of this, we have also included the average of the uncorrected and BSSE-corrected binding energies on the extrapolation plots.

Three different spin biased corrections to the MP2 calculations were performed: SCS-MP2, SCS-MI-MP2, and SOS-MP2.<sup>43-45</sup> This required *a posteriori* scaling of the same-spin and opposite-spin MP2 correlation energies according to

$$E_{spin-biased\ correction} = c_{OS}E_{OS-correlation} + c_{SS}E_{SS-correlation} \quad (2)$$

where  $c_{OS} = 1.2, 0.4, 1.3$  and  $c_{SS} = 1/3, 1.29, 0.0$  for SCS-MP2, SCS-MI-MP2, and SOS-MP2, respectively. Each of these structures (PD, T( $C_{2v}$ ), and TT( $C_s$ )) were re-optimized with each spin biased method using the plain (non-augmented) Dunning basis sets (cc- $VnZ$ ).<sup>35</sup>

All binding energies were corrected for the basis set superposition error (BSSE) following the function counterpoise method proposed by Boys and Bernardi (3).<sup>46</sup> The fragment relaxation terms<sup>47</sup> were taken into account in the calculation of the BSSE-corrected binding energies.

$$E_{AB}^{CP} = E_{AB}(AB) - E_{A,ref}(A) - E_{B,ref}(B) - ((E_A(AB) + E_B(AB)) - (E_{A,dimer}(A) + E_{B,dimer}(B))) \quad (3)$$

The parentheses specify the basis functions present in the calculation. The energies with the “ref” subscript indicate that the monomer geometry is the gas-phase optimized geometry whereas the “dimer” subscript indicates that the energies is evaluated at the geometry of that molecule in the optimized dimer configuration. All calculations were performed with the NWChem 7.0.2 electronic structure package<sup>48</sup> forcing zero linear dependencies for all basis sets.

**b. CCSD and CCSD(T) calculations:** The CCSD and CCSD(T) calculations were performed for the PD, T( $C_{2v}$ ) and TT( $C_s$ ) conformers. The PD and T( $C_{2v}$ ) structures were fully optimized with both the Dunning cc-pVDZ and cc-pVTZ basis sets (denoted as PD structures in the study of Miliordos *et. al*<sup>13</sup>). The binding energies with larger basis sets were computed at the SCS-MP2 optimized geometry.<sup>45</sup> All binding energies for the TT( $C_s$ ) conformer were computed at the SCS-MP2 optimized geometries.<sup>45</sup> The CCSD binding energies were computed at the same geometry as the CCSD(T) binding energies. The CBS values were estimated by fitting the binding energies with different basis set sizes to the double exponential (Equation 1). The extrapolation was performed for the BSSE-corrected, uncorrected, and averaged values, respectively, with the error bars assigned to encompass all 3 extrapolated CBS values for each conformer. All binding energies were corrected for the basis set superposition error (BSSE) and were performed by forcing zero linear dependencies for all basis functions, with the exception of four single point energy calculations for which there were 2 linear dependencies as noted in the results section. The CCSD and CCSD(T) calculations were performed with the NWChem 7.0.2 electronic structure package.<sup>48</sup>

**c. DFT calculations:** The DFT functionals were selected from each rung of Jacob’s ladder to compare with the CCSD(T)/CBS value for the PD and T( $C_{2v}$ ) conformers. The PD and T-shaped configurations were selected in order compare the performance of the various functional for both

the  $\pi\cdots\pi$  and  $\text{CH}\cdots\pi$  interactions. These functionals included SVWN,<sup>49–53</sup> PBE,<sup>54</sup> TPSS,<sup>55</sup> M06-L,<sup>56</sup> M11-L,<sup>57</sup> M11,<sup>58</sup> M06,<sup>59</sup> M06-2X,<sup>59</sup> B3LYP,<sup>60,61</sup> PBE0,<sup>62</sup>  $\omega$ B97-XD,<sup>63</sup> B97-D,<sup>64,65</sup> and B2PLYP<sup>66</sup>. The Grimme D3 empirical dispersion correction (where applicable) with zero damping<sup>33,34</sup> was used. The optimizations were performed using Gaussian 09<sup>67</sup> using “tight” thresholds and appropriate grid sizes to allow for convergence of the relatively flat energy landscape (super fine grid for T( $C_{2v}$ ) and ultrafine for PD). The DFT binding energies were corrected for basis set superposition error (BSSE). All binding energies were computed with the aug-cc-pVTZ basis set. The M06-L and M06 optimizations of the T2 and PD conformers were carried out with the NWChem 7.0.2 electronic structure package.<sup>48</sup> The B2PLYP and B2PLYP-D3 optimizations of the PD conformer were also carried out with the NWChem 7.0.2 electronic structure package<sup>48</sup> due to the increased computational cost associated with the addition of the PT2 correlation and the very fine grids necessary to get converged results on a flat potential energy surface.

The Cartesian coordinates of the various conformers used in the calculations are listed in Tables S4 – S6 of the SI, whereas their intramolecular distances (cf. Figure 1) at the optimized geometries obtained at various levels of theory are collected in Table 1.

### III. Results and Discussion

#### a. $\text{CH}\cdots\pi$ Energy Landscape probed at the MP2 level of theory

Szalewicz and co-workers have previously reported an extensive, 6-dimensional characterization of the benzene dimer potential energy surface (PES) analytically fitted to 491 dimer geometries obtained from symmetry adapted perturbation theory (SAPT) based on a Kohn-Sham description of the monomers<sup>15</sup> and subsequently modified to ensure better accuracy in the region of the potential minima.<sup>17</sup> The stationary points (minima, first and higher order transition states) were then determined on the fitted PES; a subset of these previously reported low-lying stationary points were used as guides in our study. We have initially optimized the T-shaped benzene dimer conformer (T,  $C_{2v}$  symmetry, see Figure 1) and computed the harmonic frequencies. For this T-shaped structure (see Table 1 for  $R_{\text{COM}}$ , the center of mass distance between the two fragments), there were two imaginary frequencies ( $i*26.2\text{ cm}^{-1}$  and  $i*13.9\text{ cm}^{-1}$ ) at the MP2/aVTZ level of theory. Following the mode of the largest imaginary frequency, we arrive at the tilted T-shape (TT,  $C_s$  symmetry) conformer. This structure has only one small imaginary frequency ( $i*6.3$

$\text{cm}^{-1}$ ) at the MP2/aVTZ level corresponding to a small out-of-plane tilt, which breaks the  $C_s$  symmetry leading to a dimer arrangement of  $C_1$  symmetry. In the previous discussion we have adopted the notation  $T(C_{2v})$  and  $TT(C_s)$  to describe the dimer configurations by the conformer designation and the symmetry. The PES becomes flatter as the basis set size increases, practically leading to a nearly isoenergetic structure between the  $TT(C_s)$  and the arrangement of  $C_1$  symmetry at the MP2/aVTZ level. For this reason, we will consider the  $TT(C_s)$  symmetry as the most favorable  $\text{CH}\cdots\pi$  interaction. Consequently, the  $T(C_{2v})$  and  $TT(C_s)$  along with the  $PD(C_{2h})$  structures will be used to assess the performance of MP2, spin biased MP2, and DFT against CCSD(T)/CBS benchmarks (section b) on  $\text{CH}\cdots\pi$  interactions.

The MP2 binding energies (kcal/mol) for the two conformers,  $T(C_{2v})$  and  $TT(C_s)$ , are listed in Table 2. The extrapolation of these binding energies to the MP2/CBS limit, shown in Figure 2, produces CBS limit values of  $-3.77 \pm 0.07$  kcal/mol and  $-3.98 \pm 0.08$  kcal/mol for the  $T(C_{2v})$  and  $TT(C_s)$  conformers, respectively. These results suggest that tilting of the benzene dimer donating the CH bond increases the interaction by  $\sim 0.2$  kcal/mol. Relative to the PD conformer (MP2/CBS:  $-5.00$  kcal/mol),<sup>13</sup> these  $\text{CH}\cdots\pi$  configurations have smaller MP2/CBS binding energies by  $\gtrsim 1$  kcal/mol. Note that previous studies<sup>10,17</sup> have reported CBS limits that underestimate the absolute magnitude of these interactions by 0.5 kcal/mol for the PD and 0.3 kcal/mol for the  $TT(C_{2v})$  arrangements either at the MP2/CBS limit<sup>10</sup> or at the MP2/aVQZ+bond functions level.<sup>17</sup> As noted earlier, the MP2 level of theory has been shown to overestimate the binding energy of the PD conformer by nearly a factor of 2.<sup>13</sup> Further, it should be noted that the BSSE-corrected results with the aug-cc-pVDZ basis set align more closely with benchmarks, thus obtaining a more accurate binding energy (with a small basis set) for the wrong reasons. Extrapolating to the CBS limit makes the agreement with benchmarks worse. However, the MP2/CBS values are useful in assessing the performance of the SOS-MP2 and SCS-MP2 corrections in reproducing the CCSD(T) results. Therefore, a comparison of the performance of MP2, the spin biased MP2 methods, and various DFT functionals compared to the CCSD(T)/CBS benchmarks for both the  $\text{CH}\cdots\pi$  ( $T$ ,  $TT$ ) and  $\pi\cdots\pi$  ( $PD$ ) interactions will be the focus of the subsequent sections.

## **b. CCSD(T) Benchmarks for the $PD(C_{2h})$ , $T(C_{2v})$ , and $TT(C_s)$ conformers**

The uncorrected and BSSE-corrected CCSD(T) binding energies are compiled in Table 3. Their extrapolation to the CCSD(T)/CBS, see Figures 3 and 4, produces values of  $-2.65 \pm 0.02$  kcal/mol for the PD( $C_{2h}$ ),  $-2.74 \pm 0.03$  kcal/mol for the T( $C_{2v}$ ), and  $-2.83 \pm 0.01$  kcal/mol for the TT( $C_s$ ) conformers, respectively. The energy differences between these conformers are small yet distinguishable within the margin of error. Interestingly, the T( $C_{2v}$ ) and TT( $C_s$ ) conformers exhibit different convergence patterns (cf. Figures 3 and 4) when extrapolated to the CBS limit. The variation of the average of the uncorrected and BSSE-corrected CCSD(T)/VDZ binding energies for the TT( $C_s$ ) conformer with basis set size is overall quite small, with the maximum deviation from the CBS value by  $\sim 0.2$  kcal/mol for all basis sets. The binding energy of the PD dimer is smaller than both T and TT conformers. The TT conformer is the lowest in energy among the 3 intermolecular arrangements, strengthening the CH $\cdots\pi$  interaction found in T( $C_{2v}$ ) by  $\sim 0.1$  kcal/mol due to the tilting of the benzene dimer donating the hydrogen-like bond. The above calculations were performed with zero linear dependencies for all basis functions, with the exception of four calculations with the cc-pV5Z basis set as noted in Table 3. The CCSD(T)/CBS binding energy for PD reported here (obtained with zero linear dependencies) is nearly identical to the one published earlier in 2014.<sup>13</sup>

Comparing these CCSD(T)/CBS benchmarks to the MP2/CBS estimates (cf. Table 2 and previous section), we find that MP2 overestimates the  $\pi\cdots\pi$  (PD) interaction<sup>13</sup> by 1.9 $\times$  and the CH $\cdots\pi$  interaction by 1.4 $\times$  with respect to the CCSD(T)/CBS benchmarks, i.e., the error is not comparable for the two bonding scenarios. This difference mainly arises from the fact that MP2 predicts PD as the global minimum by  $\geq 1$  kcal/mol compared to the T and TT arrangements, whereas CCSD(T) produces the TT as the lowest energy arrangement that lies 0.2 kcal/mol below PD. In addition, it overestimates the energy difference between the T( $C_{2v}$ ) and TT( $C_s$ ) conformers by  $\sim 2\times$ . As regards the optimized geometries, MP2 yields structures that have intermolecular separations that are  $\geq 0.2$  Å away from the CCSD(T) optimized ones for both the PD and T conformers (cf. Table 1). In general, the intermolecular distances between benzene molecules are smaller in the MP2 than in the CCSD(T) optimized structures.

Our current CCSD(T) estimates for the intermolecular distances compare favorably with a previous estimate<sup>10</sup> at the counterpoise corrected QCISD(T)/aug-cc-pVTZ level that reported  $R_1=1.715$  Å (compared to our result of 1.684 Å) for the PD conformer and  $R_{\text{COM}} = 4.989$  Å

(compared to our result of 4.950 Å) for the T conformer (cf. Table 1 for our results). They estimated QCISD(T)/CBS values for the binding energy by extrapolating the correlation energy with the aVTZ and aVQZ basis set via the formula  $E_{aVnZ}^{corr} = E_{\infty}^{corr} + a/n^3$ ,  $n = 3, 4$ , by adding the resulting from the fit  $E_{\infty}^{corr}$  to the SCF/aVQZ value. Their reported binding energy of 2.66 kcal/mol for the PD conformer is identical within our extrapolation error with our CCSD(T)/CBS estimate of 2.65 kcal/mol, while their estimate of 2.68 kcal/mol for the T conformer is just 0.06 kcal/mol lower than our CCSD(T)/CBS estimate of -2.74 kcal/mol. Similar agreement is found between our results and the ones previously reported by Szalewicz and co-workers,<sup>15,17</sup> who reported  $R_{COM} = 3.962$  Å and  $R_1 = 4.982$  Å for the PD and T conformers, respectively. Their CCSD(T) “best estimates”, computed as MP2/aug-cc-pVTZ interaction energy plus  $\Delta CCSD(T) = E_{int}^{CCSD(T)} - E_{int}^{MP2}$  obtained using the aug-cc-pVDZ basis set with both basis sets supplemented with mid bond functions, of  $-2.70 \pm 0.2$  (PD),  $-2.68$  kcal/mol (T) and  $-2.80 \pm 0.1$  kcal/mol (TT) and are within 0.05 kcal/mol from our CCSD(T)/CBS estimates (cf. Table 3) albeit the energetic order between PD and T is inconclusive within the error bars reported. Note that this is amended in a subsequent study,<sup>15</sup> in which the binding energies were revised to 2.62 (PD), 2.64 (T) and 2.75 kcal/mol (TT). Our reported binding energy for the T-shaped dimer aligns closely with the CCSD(T) estimate from Sinnokrat et. al<sup>12,68</sup> (2.74 kcal/mol) which were estimated by applying a  $\Delta CCSD(T)$  (computed with the aug-cc-pVDZ basis set) on top of an MP2/aug-cc-pVQZ calculation. However, they predict the interaction in the PD configuration to be 0.04 kcal/mol stronger than that of the T-shaped configuration, which disagrees with our results reported here. Further, the work of Hobza et. al<sup>14</sup> supports the stronger interaction in the T-shaped configuration over that of the PD configuration. However, the difference in energy they predict is  $\sim 0.33$  kcal/mol whereas our results indicate a  $\sim 0.1$  kcal/mol energy difference. Further, their reported values of 2.336 and 2.005 kcal/mol for the T-shaped and PD dimers computed with a double zeta basis set are vastly underestimated in comparison with the CBS results reported in this work.

The CCSD binding energies, listed in Table ST2 of the SI, were also found to differ significantly from the CCSD(T) results. CCSD underestimates the binding energy of each conformer with the cc-pV5Z basis set by 1.24 kcal/mol (PD), 0.68 kcal/mol (T( $C_{2v}$ )), and 0.70 kcal/mol (TT( $C_s$ )). This demonstrates the importance and significance of the triple excitations to the total binding energy, contributing between  $\sim 0.7$ -1.3 kcal/mol for the 3 conformers with the cc-pV5Z basis set. The CCSD results also vary significantly with the MP2 results (section a). The

CCSD results underestimate the binding energies (relative to CCSD(T)) whereas the MP2 results overestimate the binding energies, as previously discussed.

**c. Performance of spin biased MP2 methods (SCS-MP2, SCS-MI-MP2, SOS-MP2) for CH $\cdots$  $\pi$  and  $\pi\cdots\pi$  interactions**

The BSSE-uncorrected binding energies for the SCS-MP2, SCS-MI-MP2, and SOS-MP2 methods are listed in Table 4. These results were obtained at the optimized geometries of the various benzene dimer conformers with the respective spin biased MP2 methods. The binding energies produced by these spin biased methods are compared to the CCSD(T)/CBS benchmark values (section b) in Figure 5. The SCS-MP2 and SCS-MI-MP2 methods overestimate the relative stability of the CH $\cdots$  $\pi$  vs.  $\pi\cdots\pi$  interactions by predicting a stronger interaction in the PD relative to the T-shaped conformer. In the SOS-MP2 method, PD and TT( $C_s$ ) are nearly isoenergetic. For all spin biased methods, we observe an overall poor agreement with the CCSD(T)/CBS benchmark values (yet an improvement over MP2). It should be noted that Miliordos *et. al*<sup>13</sup> reported that the SCS-MP2 method produced accurate binding energies for the PD conformer when these are evaluated *at the MP2 optimized geometry*. However, in this study we optimize the geometries with each spin biased method and find that none of these correction schemes produce accurate binding energies at the spin biased MP2 optimized geometries. At the MP2 optimized geometries (Tables S5 and S6 of the SI), SCS-MP2 underestimates the binding energies of both the T( $C_{2v}$ ) and TT( $C_s$ ) conformers by  $\sim 0.2$  kcal/mol relative to the CCSD(T)/CBS benchmark (-2.48 vs. -2.74 kcal/mol and -2.62 vs. -2.83 kcal/mol). Rather, SCS-MI-MP2 shows a remarkable agreement with the CCSD(T)/CBS energy benchmark at the MP2 optimized geometries aligning within the margin of error.

We find that the SCS-MP2 and SCS-MI-MP2 correction schemes produce geometries that are quite similar to the CCSD(T) optimized ones and in excellent agreement with the experimentally determined  $R_{COM}$  value for the T-shaped dimer (cf. Table 1). This is true for all conformers studied with the differences between the center of masses distance (spin biased MP2 vs. CCSD(T)) not exceeding 0.017 Å and 0.013 Å for SCS-MP2 and SCS-MI-MP2, respectively. Figure 6 shows the percentage error of MP2 and its spin biased methods with respect to the CCSD(T) benchmark for both the intermolecular distance ( $x$ -axis) and the binding energy ( $y$ -axis)

of the PD ( $\pi\cdots\pi$ ) and T ( $\text{CH}\cdots\pi$ ) conformers of the benzene dimer. The ( $D_e$ ,  $R_e$ ) pairs for the PD (blue) and T (orange) conformers are connected with a straight line for each method. To this end, data pairs for distance and binding energy that are closer to (0, 0) correspond to the most accurate methods. This correlation plot clearly shows the inability of MP2 to produce both accurate intermolecular separations and binding energies. The SCS-MP2 and SCS-MI-MP2 (gray shaded boxes in Figure 5) are the two methods with ( $D_e$ ,  $R_e$ ) pairs close to (0, 0), producing very accurate geometries albeit with a maximum error of  $\sim 20\%$  in the binding energies for the PD conformer (note that these results are for the optimized geometries at the corresponding spin biased methods). Alternatively, if errors of the order of 6% in the intermolecular distances are acceptable, the SCS-MI-MP2//MP2 protocol (i.e., scaling the correlation energy at the MP2 optimized geometry) produces very accurate binding energies for both the PD and T conformers, albeit the fact that the MP2 geometries do not align closely with those at the CCSD(T) level. Given that optimizing the geometries with CCSD(T) is quite computationally expensive, SCS-MP2 and SCS-MI-MP2//MP2 offer more cost-effective alternatives to produce accurate intermolecular geometries and binding energies that are very close to those obtained by CCSD(T).

#### d. Performance of DFT functionals for C-H $\cdots\pi$ and $\pi\cdots\pi$ interactions

The uncorrected and BSSE-corrected binding energies of the PD and T benzene dimer conformers with each density functional considered in this study are organized in Table 5. In general, since DFT is not as sensitive to the size of the basis set as other wavefunction based methods, these binding energies were all computed using the aug-cc-pVTZ basis set. Note that we will use the average of the BSSE-uncorrected and -corrected values as the best estimate for the functional. The  $R_{\text{COM}}$ ,  $R_1$  and  $R_2$  distances for the DFT optimized PD and T( $C_{2v}$ ) ( $R_{\text{COM}}$  only) conformers are listed in Table 1, along with those values for the MP2 and CCSD(T) levels of theory. Note that  $R_{\text{COM}}$ ,  $R_1$  and  $R_2$  are defined in Figure 1.

As expected, the functionals without Grimme's D3 dispersion correction perform poorly, significantly underestimating the binding energies (cf. Table 5). It is important to note that without the D3 correction, the PD conformer typically optimizes to a T-shaped conformation, indicating that these methods do not yield the PD conformer as a stationary point on the PES. With the D3 correction, many of the DFT functionals produce binding energies within  $\sim 0.5$  kcal/mol of the

CCSD(T)/CBS value. This includes functionals from the relatively simple GGA rung of Jacob's ladder, up to the hybrid GGA rung (including components of exact exchange) and double hybrid rung (including components of PT2 correlation). Figure 7 traces the absolute values of the intermolecular distances (top panel) and the average of the uncorrected and BSSE-corrected binding energies (bottom panel) for the PD and T conformers obtained with the various DFT functionals and their comparison to the CCSD(T) benchmarks. Their percentage error with respect to the CCSD(T) benchmarks is shown in Figure 8. In both Figures 7 and 8 the DFT functionals are ordered in the  $x$ -axis from left to right according to their position on Jacob's ladder, i.e., their increasing complexity. As can be seen from Figure 8, there is no clear trend of increased accuracy of the functionals with increasing their complexity (higher position on Jacob's ladder). A similar plot when the functionals are ordered in the  $x$ -axis according to their total unsigned error for both conformers is shown in figure SF1 of the SI. Finally, Figure 9 shows the percentage error of the 5 best functionals for intermolecular distances and the 5 best ones for binding energy with respect to the CCSD(T) benchmark, similar to the one presented earlier in Figure 6 for the MP2 and its spin biased methods. The functionals that perform well for both CH $\cdots\pi$  and  $\pi\cdots\pi$  bonding scenarios include TPSS-D3, B3LYP-D3, B97-D, B97-D3, and B2PLYP-D3 (see Figure SF1 and SF2 of the SI for the ordering of the functionals according to the total unsigned error for the energetics and structure, respectively). Using these functionals resulted in the smallest combined error for the PD and T( $C_{2v}$ ) dimers. In addition, each of these functionals produced binding energies within 6% of the CCSD(T)/CBS values for both the CH $\cdots\pi$  and the  $\pi\cdots\pi$  bonding scenarios.

Ideally, a DFT functional that works well for both the CH $\cdots\pi$  and the  $\pi\cdots\pi$  and bonding scenarios (represented by the PD and T( $C_{2v}$ ) dimer) is desired. It is important for this functional to reasonably reproduce the magnitude of the interactions in addition to the relative strength. That said, according to the CCSD(T)/CBS results, the CH $\cdots\pi$  interaction should be slightly more favorable than the  $\pi\cdots\pi$  interaction. All top-performing functionals successfully reproduce the relative ordering of these two bonding scenarios. In addition, we see good agreement between the DFT optimized geometries and the CCSD(T)-optimized geometries for these functionals (Table 1). In general, the T( $C_{2v}$ ) structures optimized with the functionals with the D3 dispersion correction (when applicable), show good agreement with the CCSD(T) optimized ones, all lying within 0.09 Å for the  $R_{\text{COM}}$  (except for SVWN, which deviates by 0.21 Å). The  $R_{\text{COM}}$  values from the M11-L, PBE0-D3, B3LYP-D3, B97-D3,  $\omega$ B97XD, B2PLYP-D3-optimized structures are all

within  $\sim 0.03$  Å. The  $\omega$ B97XD, M11, M06-2x-D3, and B2PLYP-D3 functionals most closely reproduce the structures of the CCSD(T)-optimized PD structures, deviating by  $< 0.09$  Å for either  $R_1$ ,  $R_2$ , and  $R_{\text{COM}}$ . However, many of the DFT functionals that most accurately predict the binding energies (TPSS-D3, B3LYP-D3, B97-D) tend to overestimate the  $R_1$  and  $R_2$  distances by up to 0.10 Å. Out of the best-performing functionals (on the energetics), the B2PLYP-D3 functional most closely aligns with the  $R_1$ ,  $R_2$ , and  $R_{\text{COM}}$  values of the CCSD(T) optimized geometries, overestimating the distances by only 0.013 Å, 0.025 Å, and 0.017 Å, respectively. Additionally, the B97-D3 functional overestimates the  $R_1$ ,  $R_2$ , and  $R_{\text{COM}}$  values of the CCSD(T) geometries by 0.105 Å, 0.028 Å, and 0.072 Å, respectively, but performs slightly better on the energetics than B2PLYP-D3. Based on the previous discussion and the combined results shown in Figure 9, we recommend the B97-D3 and B2PLYP-D3 functionals as the best choices for reproducing both the absolute binding energies and the geometries of the CCSD(T) benchmarks. Out of the previous two, B2PLYP-D3 also best reproduces the relative energies of the two conformers that correspond to the two different bonding scenarios. It is encouraging that this functional is at the top of Jacob's ladder among the set of functionals we considered in this study.

Despite the B2PLYP functional (at the top of Jacob's ladder) performing most accurately, we do not generally see a systematic improvement as Jacob's ladder is ascended. We draw attention to the functionals that are related to one another at various rungs of Jacob's ladder. These include the PBE $\rightarrow$ PBE0, M11-L $\rightarrow$ M11, and M06-L $\rightarrow$ M06, M06-2x sets of functionals. The PBE0 functional yields only a modest improvement over PBE on the structural and energetic errors for both conformers. The M11 functional improves upon the M11-L functional in the structure but performs worse in its estimation of the binding energies. Lastly, the M06 and M06-2x functionals perform more accurately on the binding energies compared to M06-L but worse on the optimized intermolecular distances. That said, it is not guaranteed that a more complex (higher on Jacob's ladder) functional will yield more accurate results for these interactions. This emphasizes the importance of benchmarking DFT functionals against the gold standard CCSD(T)/CBS calculations to establish their reliability for a given type of interaction type and system.

#### IV. Conclusions

We have explored the potential energy landscape of the benzene dimer and established CCSD(T)/CBS binding energies of  $-2.65 \pm 0.02$  kcal/mol for the PD( $C_{2h}$ ),  $-2.74 \pm 0.03$  kcal/mol for the T( $C_{2v}$ ), and  $-2.83 \pm 0.01$  kcal/mol for the TT( $C_s$ ) conformers. The first corresponds to a  $\pi \cdots \pi$ , whereas the last two to a CH $\cdots\pi$  interaction, with the T conformer being a transition state. The TT( $C_s$ ) arrangement is the lowest energy conformer, in which the benzene molecule donating the CH bond is slightly (by  $\sim 0.2$  kcal/mol at the MP2 level of theory) tilted. To this end, the CH $\cdots\pi$  (T-shaped) interactions are only slightly more favorable than the strongest  $\pi \cdots \pi$  interaction (PD), with the difference being  $< 0.1$  kcal/mol (including the margin of error). Despite the fact that CCSD(T)/CBS computations are considered the current gold standard, the significance of the triple excitations to the total correlation energy ( $\sim 0.7 - 1.3$  kcal/mol with the cc-pV5Z basis set) brings into question whether quadruple (or higher) excitations might also be necessary. Importantly, a recent study aimed at providing CCSDT(Q) benchmarks for the PD orientation found that the full treatment of the triple excitations with perturbative quadruple excitations led to a destabilization of  $\sim 0.058$  kcal/mol of the total binding energy.<sup>26</sup> Thus, the contributions from the quadruple excitations are relatively small and do not alter the conclusions drawn in this work. These results, together with the corresponding intermolecular distances, serve as benchmarks to assess the accuracy of lower scaling methods such as MP2 and its spin biased variants as well as several DFT functionals on different rungs of Jacob's ladder.

As previously shown by Miliordos *et al.*,<sup>13</sup> the MP2 level of theory produces inaccurate energetics for the  $\pi \cdots \pi$  interactions in the benzene dimer and this is also the case for the CH $\cdots\pi$  interactions. MP2 overestimates the binding energies for all conformers by  $1.4\times - 1.9\times$  and produces a  $\sim 1$  kcal/mol energy difference between the nearly isoenergetic PD and T conformers. The spin biased corrections to the MP2 energy amend, to some extent, this disagreement. When the geometries are optimized with the spin biased methods, all methods incorrectly predict that the PD conformer has a stronger interaction than the T( $C_{2v}$ ) one. While SCS-MP2 has been shown to perform well with the PD conformer at the MP2 optimized geometry, we find that this was an artifact of the geometry used to perform the spin correction. When the dimer is re-optimized with the SCS-MP2 method (rather than adding the spin corrections at the MP2 optimized geometry) the errors with respect to CCSD(T) are much larger. However, we find that the SCS-MP2 and SCS-MI-MP2 optimized geometries closely resemble those obtained at the CCSD(T) level of theory, a fact that offers a more cost-effective method to predict the structures obtained at a higher level of

theory. In addition, when the SCS-MI-MP2 energy is computed *at the MP2 optimized geometry*, we find remarkable agreement with the CCSD(T)/CBS benchmarks presented in this study. The shortcomings of these available methods on the benzene dimer call for the development of alternative scaling methods capable of reproducing both the geometry and binding energy obtained with these high-level methods.

A handful of DFT functionals show promising results for reproducing both the intermolecular structures and energetics of the two benzene dimer conformers (PD and T-shaped) corresponding to the two bonding scenarios. As shown by others, the Grimme empirical dispersion correction is paramount in the description of dispersion forces, which dominate the benzene dimer energy landscape. Without this correction the parallel displaced stationary point would not exist, and the energy of the T conformer would be significantly underestimated (only a few tenths of a kcal/mol). With the dispersion correction, many functionals perform quite well for both bonding arrangements. The functionals that perform the best include TPSS-D3, B3LYP-D3, B97-D, B97-D3, and B2PLYP-D3, producing binding energies within 6% of the estimated CCSD(T)/CBS values for both the PD( $C_{2h}$ ) and T( $C_{2v}$ ) conformers. In addition, all functionals correctly predict that the T-shaped conformer exhibiting CH $\cdots\pi$  interactions is more strongly bound than the PD conformer exhibiting  $\pi\cdots\pi$  interactions (results obtained with the aug-cc-pVTZ basis set). Because the B2PLYP-D3 optimized geometries are closely aligned with those of CCSD(T), this functional is recommended for accurately describing CH $\cdots\pi$  and  $\pi\cdots\pi$  interactions with the caveat that this work represents a modest scope of available functionals and dispersion corrections, only considering the Grimme D3 correction with 13 different functionals. That said, while several MP2 spin biased methods and DFT functionals show promise, they should undergo further tests on larger system sizes to ensure the transferability of these methods to dimers of larger aromatic molecules. The availability of the CCSD(T) benchmarks reported in this study can aid further development in these areas.

**Acknowledgment:** K.M.H. acknowledges support from the Mickey and Karen Schurr Endowed Fund in Chemistry at the University of Washington. This work was supported by the US Department of Energy, Office of Science, Office of Basic Energy Sciences, Division of Chemical Sciences, Geosciences and Biosciences. Pacific Northwest National Laboratory (PNNL) is a multi-

program national laboratory operated for DOE by Battelle. A portion of the research was performed using EMSL (grid.436923.9), a DOE Office of Science User Facility sponsored by the Office of Biological and Environmental Research. Part of this work were performed using the Ilahie cluster, which was purchased using funds from a Major Research Instrumentation (MRI) grant from the National Science Foundation (CHE-1624430). This work was also facilitated using advanced computational, storage, and networking infrastructure provided by the Hyak supercomputer system and funded by the Student Technology Fund at the University of Washington. This research also used resources of the National Energy Research Scientific Computing Center, which is supported by the Office of Science of the U.S. Department of Energy under Contract No. DE-AC02-05CH11231.

#### ASSOCIATED CONTENT

**Supporting Information.** Percent error of DFT functionals against CCSD(T)/CBS for intermolecular distances and binding energies ordered by total unsigned error, Cartesian coordinates for PD( $C_{2h}$ ) and T( $C_{2v}$ ) optimized at the CCSD(T)/VTZ level of theory, Cartesian coordinates for TT( $C_s$ ) optimized at the SCS-MP2/VTZ level of theory, CCSD binding energies, and spin biased MP2 energies computed at the MP2-optimized geometries. This information is available free of charge via the Internet at <http://pubs.acs.org>

**Table 1.** The  $R_{\text{COM}}$ ,  $R_1$ , and  $R_2$  distances of the optimized PD and T( $C_{2v}$ ) benzene dimer geometries at the MP2, CCSD, CCSD(T), and DFT level of theory with the triple zeta basis sets (either aug-cc-pVTZ or cc-pVTZ) and a comparison to the experimentally determined value for the T-shaped dimer (only). “N/A” indicates that the structure was not a stationary point and changed conformation upon optimization for that level of theory.

	Method	T( $C_{2v}$ )	PD		
		$R_{\text{COM}}$	$R_1$	$R_2$	$R_{\text{COM}}$
Experiment	N/A	4.96 <sup>a</sup>	N/A	N/A	N/A
Benchmark	CCSD(T)	<b>4.950</b>	<b>1.684<sup>b</sup></b>	<b>3.451<sup>b</sup></b>	<b>3.840<sup>b</sup></b>
MP2 and spin biased methods	MP2	4.770	1.559 <sup>b</sup>	3.266 <sup>b</sup>	3.619 <sup>b</sup>
	SCS-MP2	4.960	1.641	3.452	3.823
	SCS-MI-MP2	4.937	1.681	3.457	3.844
	SOS-MP2	4.960	1.707	3.534	3.925
DFT	SVWN	4.741	1.718	3.275	3.698
	PBE	5.377	N/A	N/A	N/A
	PBE-D3	5.044	1.799	3.592	4.017
	TPSS	5.705	N/A	N/A	N/A
	TPSS-D3	5.024	1.755	3.557	3.966
	M06-L	4.901	1.616	3.512	3.866
	M11-L	4.953	1.544	3.536	3.858
	B3LYP	5.697	N/A	N/A	N/A
	B3LYP-D3	4.982	1.782	3.511	3.938
	PBE0	5.310	N/A	N/A	N/A
	PBE0-D3	4.977	1.813	3.557	3.993
	B97-D	4.906	1.789	3.481	3.914
	B97-D3	4.942	1.789	3.479	3.912
	$\omega$ B97XD	4.984	1.636	3.467	3.834
	M11	4.914	1.667	3.425	3.809
	M06	4.966	1.902	3.491	3.975
	M06-2x	4.911	1.620	3.402	3.768
	M06-2x-D3	4.912	1.632	3.405	3.776
	B2PLYP	5.152	2.120	3.772	4.327
	B2PLYP-D3	4.941	1.671	3.476	3.857

<sup>a</sup> Arunan and Gutowski 1993.<sup>69</sup>

<sup>b</sup> Miliordos *et. al* 2014.<sup>13</sup>

**Table 2.** The binding energies (kcal/mol) computed at the MP2 level of theory for the T( $C_{2v}$ ) and TT( $C_s$ ) conformers with the aug-cc-pV $n$ Z ( $n = 2, 3, 4, 5$ ) basis sets. The BSSE-corrected ( $D_e^{CP}$ ) and uncorrected ( $D_e$ ) binding energies are listed for each basis set in addition to the estimated value at the complete basis set (CBS) limit.

Basis set	T( $C_{2v}$ )			TT( $C_s$ )		
	$D_e$	$D_e^{CP}$	Average	$D_e$	$D_e^{CP}$	Average
aug-cc-pVDZ	-6.799	-2.846	-4.823	-6.995	-2.994	-4.995
aug-cc-pVTZ	-4.961	-3.395	-4.178	-5.108	-3.548	-4.328
aug-cc-pVQZ	-4.083	-3.548	-3.816	-4.251	-3.704	-3.978
aug-cc-pV5Z	-4.081 <sup>a</sup>	-3.688 <sup>a</sup>	-3.885	-4.319 <sup>a</sup>	-3.886 <sup>a</sup>	-4.103
CBS		-3.77 ± 0.07			-3.98 ± 0.08	

<sup>a</sup> At the MP2/aVQZ optimized geometry

**Table 3.** The binding energies (kcal/mol) computed at the CCSD(T) level for the benzene dimer conformers. The BSSE-corrected ( $D_e^{CP}$ ) and uncorrected ( $D_e$ ) values are listed for each basis set in addition to the estimated binding energy at the complete basis set (CBS) limit.

Basis set	PD			T(C <sub>2v</sub> )			TT(C <sub>s</sub> )		
	$D_e$	$D_e^{CP}$	Average	$D_e$	$D_e^{CP}$	Average	$D_e$	$D_e^{CP}$	Average
cc-pVDZ	-2.262	-0.190	-1.226	-2.927	-0.061	-1.494	-2.913	-2.319	-2.616
cc-pVTZ	-2.899	-1.706	-2.303	-2.940	-1.749	-2.345	-2.986	-2.495	-2.741
cc-pVQZ	-2.745	-2.222	-2.484	-2.800	-2.337	-2.569	-2.908	-2.656	-2.782
cc-pV5Z	-2.730	-2.546	-2.638	-2.744 <sup>a</sup>	-2.658 <sup>a</sup>	-2.701	-2.853 <sup>a</sup>	-2.803 <sup>a</sup>	-2.828
CBS	-2.65 ± 0.02			-2.74 ± 0.03			-2.83 ± 0.01		

<sup>a</sup> Two linear dependencies.

**Table 4.** The uncorrected ( $D_e$ ) binding energies (kcal/mol) from the spin biased (SCS-MP2, SCS-MI-MP2, SOS-MP2) MP2 methods for the PD,  $^{13}\text{T}(C_{2v})$ , and TT( $C_s$ ) conformers with the cc-pVnZ ( $n = 2, 3, 4, 5$ ) basis sets.

Basis set	PD			$\text{T}(C_{2v})$			TT( $C_s$ )		
	SCS	SCS-MI	SOS	SCS	SCS-MI	SOS	SCS	SCS-MI	SOS
cc-pVDZ	-2.651	-2.540	-1.968	-2.839	-2.936	-2.419	-2.913	-2.991	-2.470
cc-pVTZ	-3.048	-3.241	-2.440	-2.822	-2.970	-2.326	-2.914	-3.046	-2.393
cc-pVQZ	-3.122	-3.211	-2.268	-2.702	-2.907	-2.193	-2.790	-2.985	-2.255
cc-pV5Z	-3.001	-3.141	-2.155	-2.574	-2.808	-2.070	-2.666	-2.891	-2.144
CCSD(T)/CBS	<b>-2.65 ± 0.02</b>			<b>-2.74 ± 0.03</b>			<b>-2.83 ± 0.01</b>		

**Table 5.** The uncorrected ( $D_e$ ) and BSSE corrected ( $D_e^{\text{CP}}$ ) binding energies (kcal/mol) of the T( $C_{2v}$ ) and PD dimers using various DFT functionals with the aug-cc-pVTZ basis set. “N/A” indicates that the structure was not a stationary point and changed conformation upon optimization.

DFT category	Functional	PD			T( $C_{2v}$ )		
		$D_e$	$D_e^{\text{CP}}$	Average	$D_e$	$D_e^{\text{CP}}$	Average
<i>LDA</i>	SVWN	-3.13	-2.92	<b>-3.03</b>	-3.57	-3.37	<b>-3.47</b>
<i>GGA</i>	PBE	N/A	N/A	<b>N/A</b>	-0.86	-0.74	<b>-0.80</b>
	PBE-D3	-2.88	-2.73	<b>-2.81</b>	-2.88	-2.73	<b>-2.81</b>
<i>Meta-GGA</i>	TPSS	N/A	N/A	<b>N/A</b>	-0.50	-0.41	<b>-0.46</b>
	TPSS-D3	-2.84	-2.69	<b>-2.77</b>	-2.86	-2.72	<b>-2.79</b>
	M06-L	-2.77	-1.86	<b>-2.32</b>	-2.27	-1.51	<b>-1.89</b>
	M11-L	-2.96	-2.03	<b>-2.50</b>	-1.99	-1.11	<b>-1.55</b>
<i>Hybrid GGA</i>	B3LYP	N/A	N/A	<b>N/A</b>	-0.20	-0.11	<b>-0.16</b>
	B3LYP-D3	-2.75	-2.58	<b>-2.67</b>	-2.94	-2.77	<b>-2.86</b>
	PBE0	N/A	N/A	<b>N/A</b>	-0.88	-0.75	<b>-0.82</b>
	PBE0-D3	-2.76	-2.59	<b>-2.68</b>	-3.00	-2.84	<b>-2.92</b>
	$\omega$ B97xD	-3.39	-3.16	<b>-3.28</b>	-3.08	-2.87	<b>-2.98</b>
	B97-D	-2.75	-2.58	<b>-2.67</b>	-2.95	-2.77	<b>-2.86</b>
	B97-D3	-2.68	-2.51	<b>-2.60</b>	-2.97	-2.79	<b>-2.88</b>
<i>Hybrid Meta GGA</i>	M11	-2.11	-1.28	<b>-1.70</b>	-2.28	-1.57	<b>-1.93</b>
	M06	-2.40	-1.70	<b>-2.05</b>	-1.98	-1.38	<b>-1.68</b>
	M06-2x	-2.61	-2.29	<b>-2.45</b>	-2.43	-2.16	<b>-2.30</b>
	M06-2x D3	-3.12	-2.81	<b>-2.97</b>	-2.88	-2.61	<b>-2.75</b>
<i>Double Hybrid</i>	B2PLYP	-0.72	-0.34	<b>-0.53</b>	-1.42	-1.01	<b>-1.22</b>
	B2PLYP-D3	-2.98	-2.45	<b>-2.72</b>	-3.14	-2.65	<b>-2.90</b>
CCSD(T)/CBS		-2.65 $\pm$ 0.02			-2.74 $\pm$ 0.03		

**Figure 1.** The geometries of the PD, T( $C_{2v}$ ), and TT( $C_s$ ) configurations of the benzene dimer. The  $R_{COM}$ ,  $R_1$ , and  $R_2$  are depicted on the PD and T( $C_{2v}$ ) structures, corresponding to the values in Table 1. The  $\times$ 's denote the center of mass (COM) of the benzene molecules.

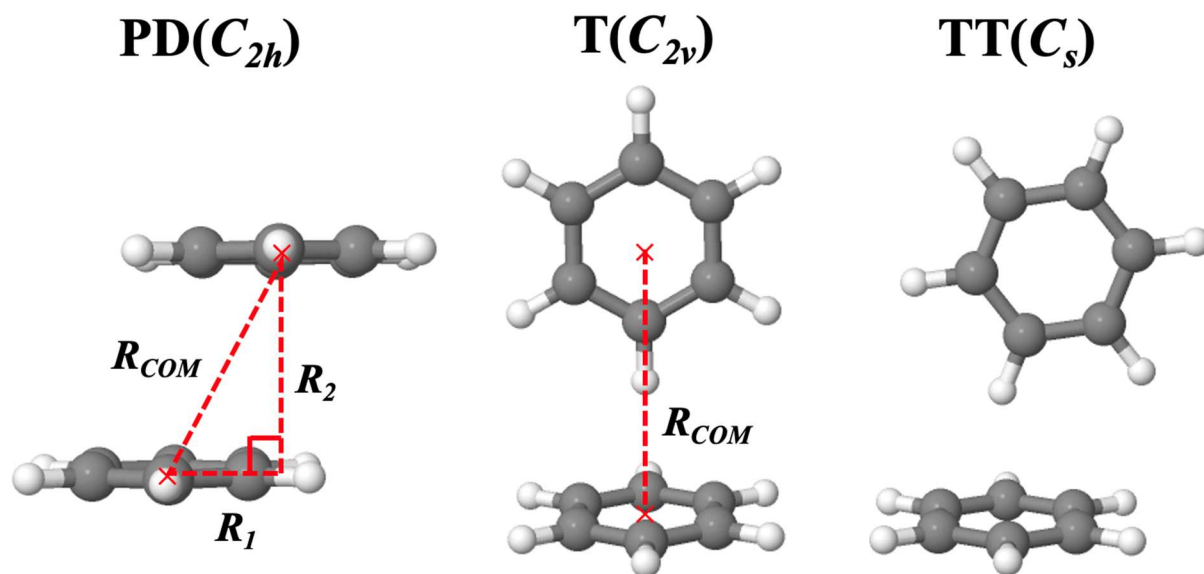


**Figure 2.** Convergence of the MP2 energies (kcal/mol) to the CBS limit (shown as the shaded area) for the T( $C_{2v}$ ) (left panel) and TT( $C_s$ ) (right panel) conformers. The figure shows the uncorrected, BSSE-corrected, and their average with the aug-cc-pVnZ,  $n=D, T, Q, 5$ , basis sets.

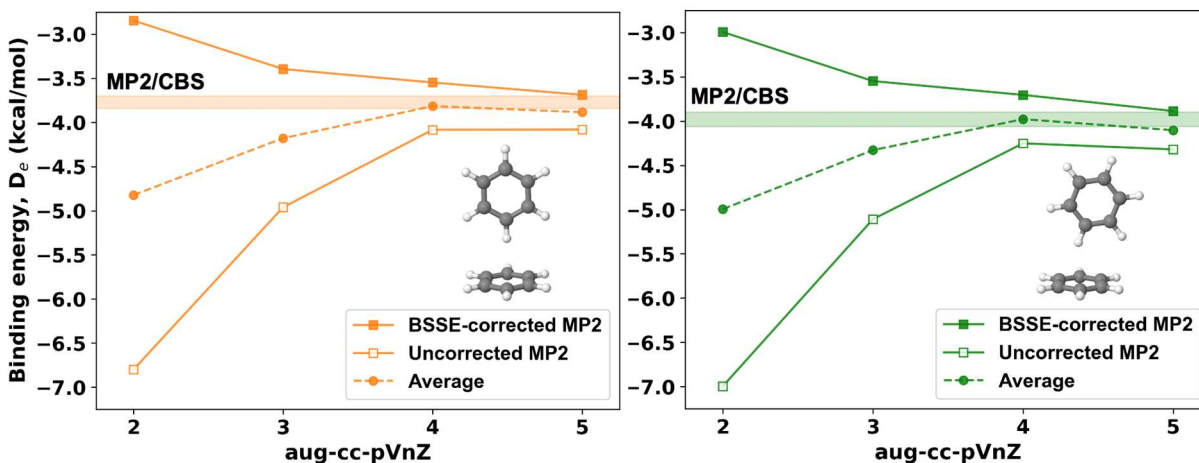


**Figure 3.** Convergence of the CCSD(T) binding energies (kcal/mol) to the CBS limit (shown as the shaded area) for the PD( $C_{2h}$ ), T( $C_{2v}$ ), and TT( $C_s$ ) conformers. The figure shows the uncorrected, BSSE-corrected, and their average with the cc-pVnZ,  $n = 2, 3, 4, 5$ , basis sets.

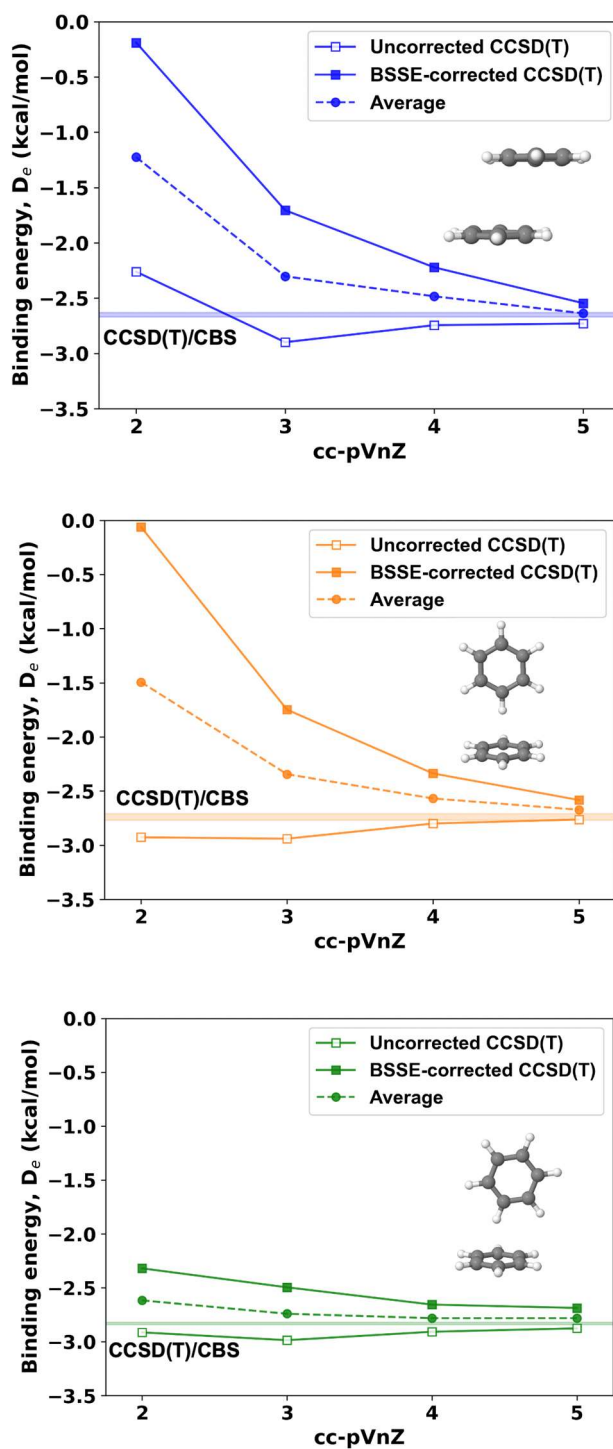


**Figure 4.** The convergence of the average of the uncorrected and BSSE-corrected CCSD(T) binding energies (kcal/mol) for the PD, T( $C_{2v}$ ), and TT( $C_s$ ) conformers with the cc-pVnZ,  $n=D, T, Q, 5$ , basis sets to the CCSD(T)/CBS limit. The dashed line traces the extrapolation to the CBS value fitted to Equation (1).

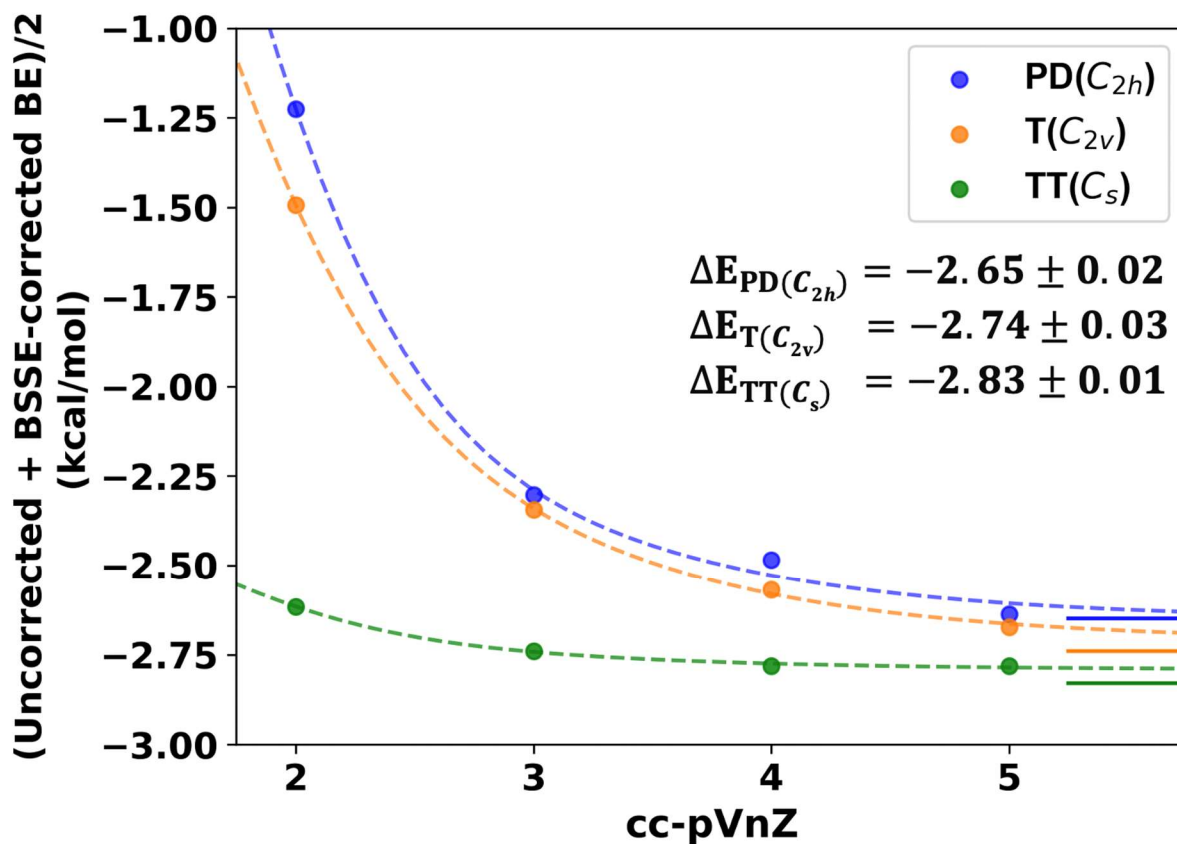


**Figure 5.** Binding energies (kcal/mol) of the PD, T and TT conformers with the spin biased corrections to MP2 with the cc-pVnZ,  $n=D, T, Q, 5$ , basis sets (raw data in Table 4): SCS-MP2 (top), SCS-MI-MP2 (middle), and SOS-MP2 (bottom) at the optimized geometries with the respective spin biased MP2 methods and their comparison to the CCSD(T)/CBS benchmarks indicated by the shaded regions.

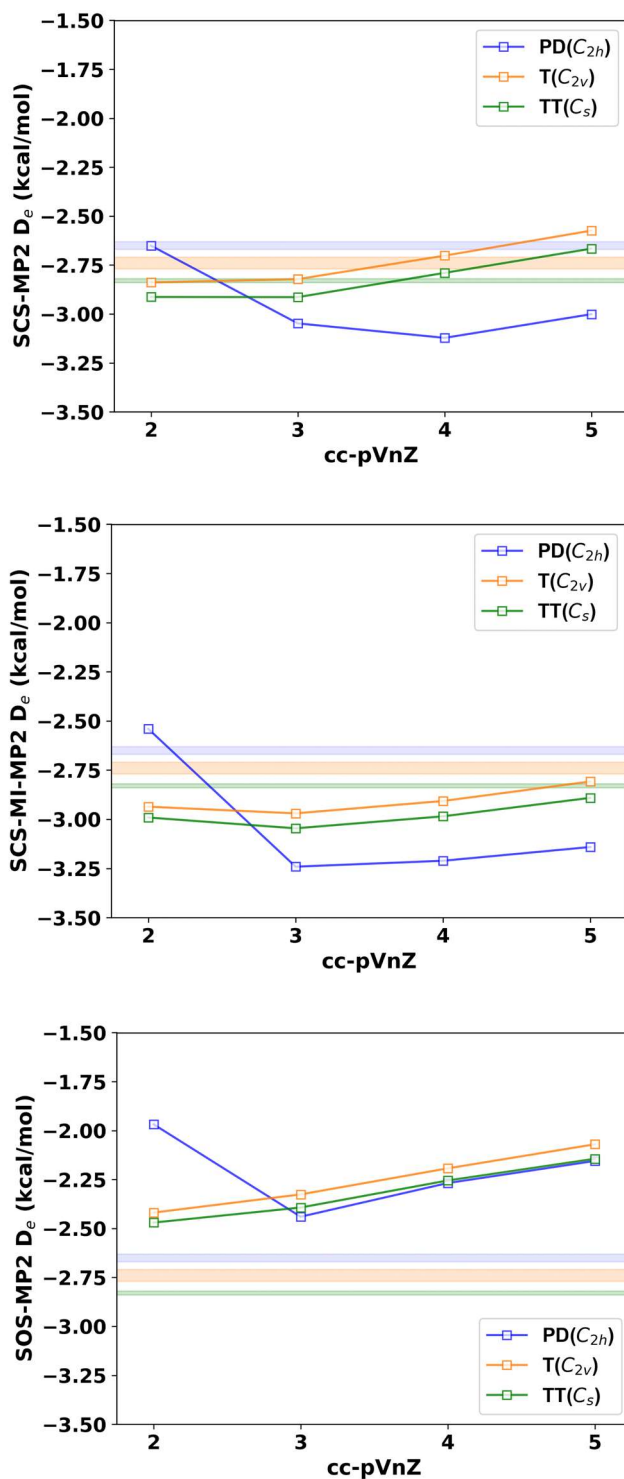


**Figure 6.** Percentage error with respect to the CCSD(T) benchmark for the intermolecular distance ( $x$ -axis) and binding energy ( $y$ -axis) of MP2 and its spin biased methods SCS-MP2, SCS-MI-MP2, SOS-MP2 for the PD ( $\pi\cdots\pi$ ) and T ( $\text{CH}\cdots\pi$ ) conformers of the benzene dimer. For the spin biased methods results are shown both at their optimized geometry (filled symbols) and at the MP2 optimized geometry (open symbols). ( $R$ ,  $E$ ) pairs that are closer to (0, 0) indicate the most accurate methods compared to CCSD(T).

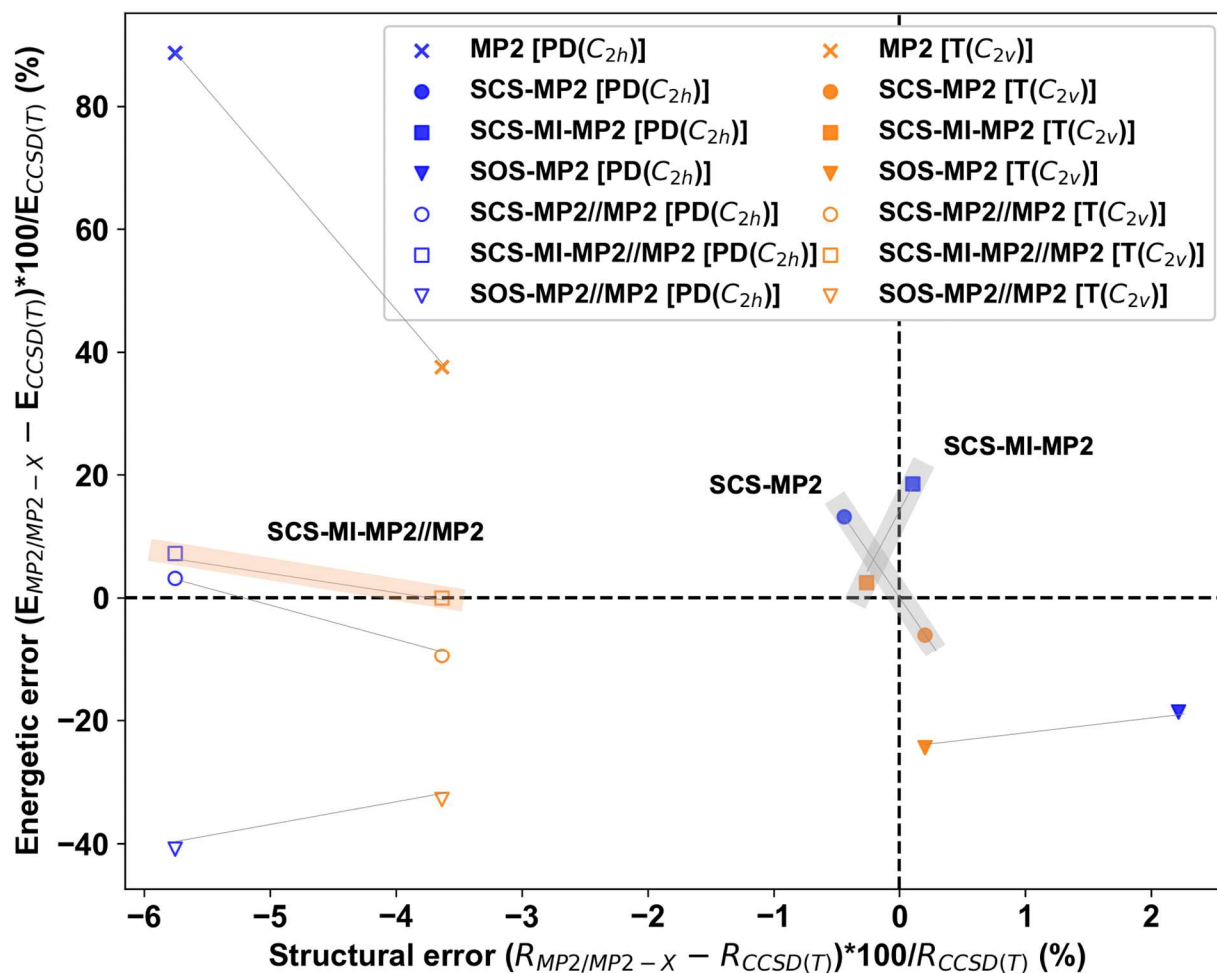


**Figure 7.** Intermolecular distances (top panel) and average of uncorrected and BSSE-corrected binding energies (bottom panel) for the PD (blue) and T (orange) conformers obtained with the various DFT functionals with the aug-cc-pVTZ basis set and comparison with the CCSD(T) benchmarks (broken lines in top panel and colored bands in bottom panel). The DFT functionals are ordered in the  $x$ -axis from left to right according to their position on Jacob's ladder.

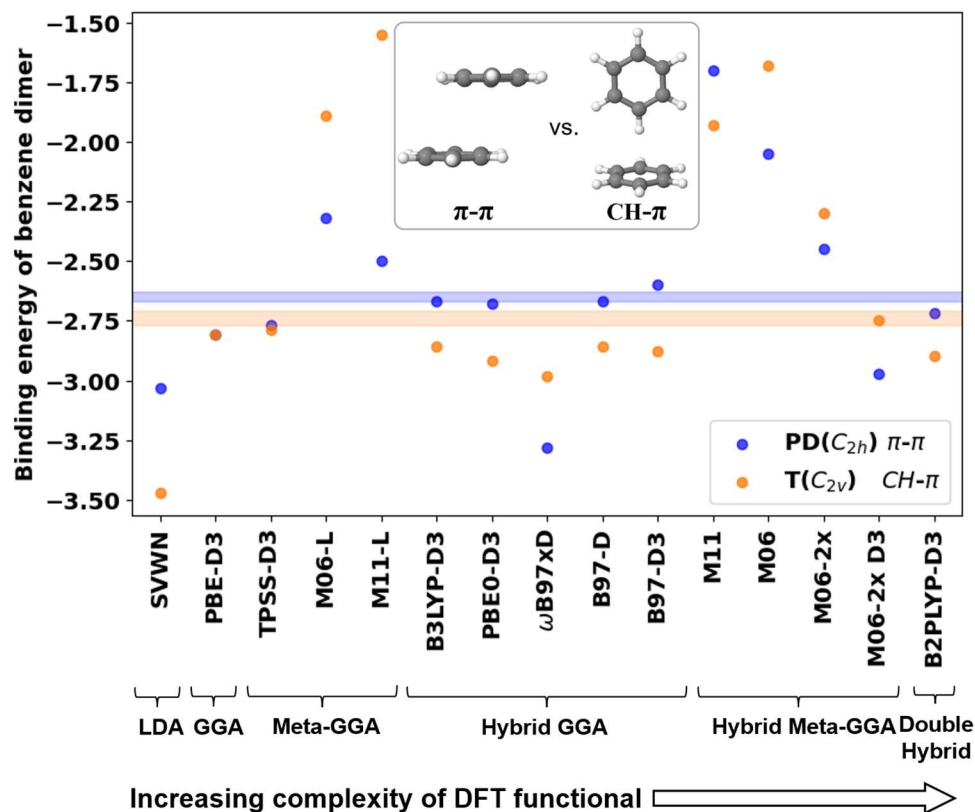


**Figure 8.** Percent error of the intermolecular distances (top panel) and binding energies (bottom panel) for the PD and T conformers with the DFT functionals compared to the CCSD(T) benchmark. The labeling of data points according to the scheme used in Figure 6. The DFT functionals are ordered in the  $x$ -axis from left to right according to their position on Jacob's ladder.

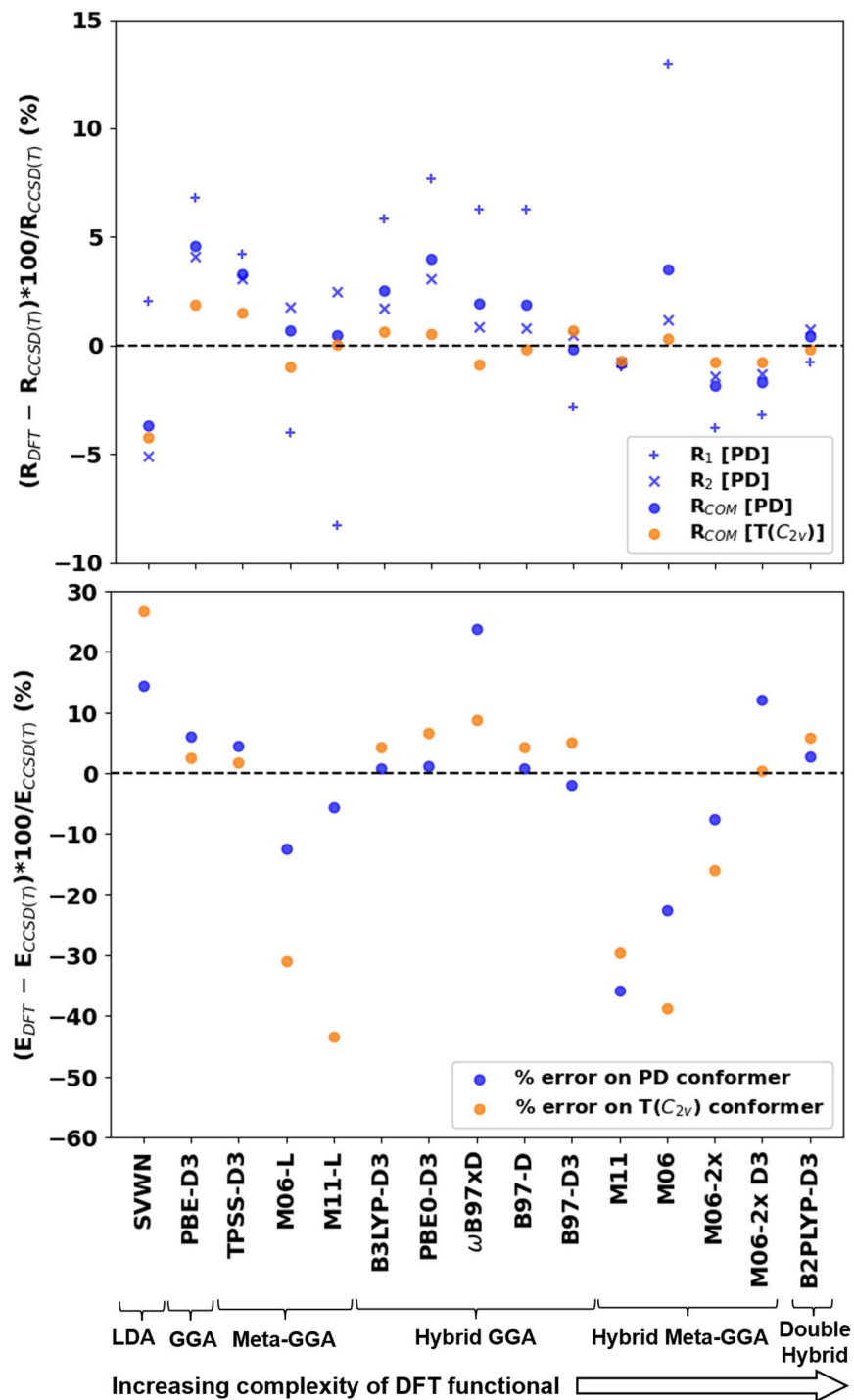
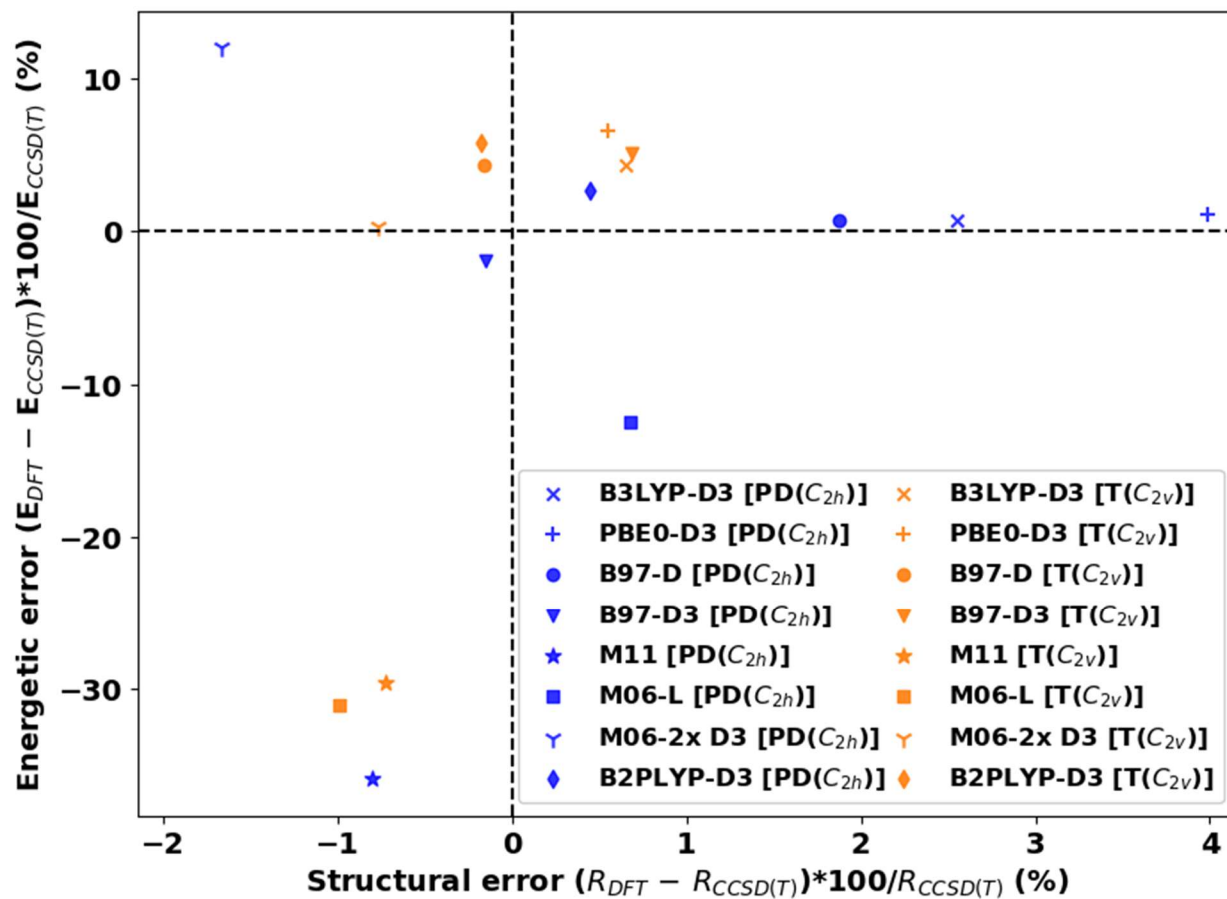


**Figure 9.** Percentage error with respect to the CCSD(T) benchmark for the intermolecular distance ( $x$ -axis) and binding energy ( $y$ -axis) of the various DFT functionals for the PD ( $\pi\cdots\pi$ ) and T ( $\text{CH}\cdots\pi$ ) conformers of the benzene dimer. ( $R$ ,  $E$ ) pairs that are closer to (0, 0) indicate the most accurate functionals compared to CCSD(T).



**References:**

- (1) Kumar, M.; Balaji, P. V. C-H... $\pi$  Interactions in Proteins: Prevalence, Pattern of Occurrence, Residue Propensities, Location, and Contribution to Protein Stability. *J. Mol. Model.* **2014**, *20* (2), 2136. <https://doi.org/10.1007/s00894-014-2136-5>.
- (2) Nishio, M.; Umezawa, Y.; Fantini, J.; Weiss, M. S.; Chakrabarti, P. CH- $\pi$  Hydrogen Bonds in Biological Macromolecules. *Phys Chem Chem Phys* **2014**, *16* (25), 12648–12683. <https://doi.org/10.1039/C4CP00099D>.
- (3) Brandl, M.; Weiss, M. S.; Jabs, A.; Sühnel, J.; Hilgenfeld, R. C-H... $\pi$ -Interactions in Proteins. *J. Mol. Biol.* **2001**, *307* (1), 357–377. <https://doi.org/10.1006/jmbi.2000.4473>.
- (4) Wang, J.; Yao, L. Dissecting C-H... $\pi$  and N-H... $\pi$  Interactions in Two Proteins Using a Combined Experimental and Computational Approach. *Sci. Rep.* **2019**, *9* (1), 20149. <https://doi.org/10.1038/s41598-019-56607-4>.
- (5) Cohen, M.; Reichmann, D.; Neuvirth, H.; Schreiber, G. Similar Chemistry, but Different Bond Preferences in Inter versus Intra-Protein Interactions. *Proteins Struct. Funct. Bioinforma.* **2008**, *72* (2), 741–753. <https://doi.org/10.1002/prot.21960>.
- (6) Spiwok, V. CH/ $\pi$  Interactions in Carbohydrate Recognition. *Molecules* **2017**, *22* (7), 1038. <https://doi.org/10.3390/molecules22071038>.
- (7) V. Balaji, P. Contribution of C-H... $\pi$  Interactions to the Affinity and Specificity of Carbohydrate Binding Sites. *Mini-Rev. Org. Chem.* **2011**, *8* (3), 222–228. <https://doi.org/10.2174/157019311796197355>.
- (8) Carter-Fenk, K.; Herbert, J. M. Reinterpreting  $\pi$ -Stacking. *Phys. Chem. Chem. Phys.* **2020**, *22* (43), 24870–24886. <https://doi.org/10.1039/D0CP05039C>.
- (9) Carter-Fenk, K.; M. Herbert, J. Electrostatics Does Not Dictate the Slip-Stacked Arrangement of Aromatic  $\pi$ - $\pi$  Interactions. *Chem. Sci.* **2020**, *11* (26), 6758–6765. <https://doi.org/10.1039/D0SC02667K>.
- (10) Janowski, T.; Pulay, P. High Accuracy Benchmark Calculations on the Benzene Dimer Potential Energy Surface. *Chem. Phys. Lett.* **2007**, *447* (1), 27–32. <https://doi.org/10.1016/j.cplett.2007.09.003>.
- (11) Park, Y. C.; Lee, J. S. Accurate Ab Initio Binding Energies of the Benzene Dimer. *J. Phys. Chem. A* **2006**, *110* (15), 5091–5095. <https://doi.org/10.1021/jp0582888>.
- (12) Sinnokrot, M. O.; Valeev, E. F.; Sherrill, C. D. Estimates of the Ab Initio Limit for  $\Pi$ - $\pi$  Interactions: The Benzene Dimer. *J. Am. Chem. Soc.* **2002**, *124* (36), 10887–10893. <https://doi.org/10.1021/ja025896h>.
- (13) Miliordos, E.; Aprà, E.; Xantheas, S. S. Benchmark Theoretical Study of the  $\pi$ - $\pi$  Binding Energy in the Benzene Dimer. *J. Phys. Chem. A* **2014**, *118* (35), 7568–7578. <https://doi.org/10.1021/jp5024235>.
- (14) Hobza, P.; Selzle, H. L.; Schlag, E. W. Potential Energy Surface for the Benzene Dimer. Results of *Ab Initio* CCSD(T) Calculations Show Two Nearly Isoenergetic Structures: T-Shaped and Parallel-Displaced. *J. Phys. Chem.* **1996**, *100* (48), 18790–18794. <https://doi.org/10.1021/jp961239y>.
- (15) Avoird, A. van der; Podeszwa, R.; Szalewicz, K.; Leforestier, C.; Harrevelt, R. van; R. Bunker, P.; Schnell, M.; Helden, G. von; Meijer, G. Vibration–Rotation–Tunneling States of the Benzene Dimer: An Ab Initio Study. *Phys. Chem. Chem. Phys.* **2010**, *12* (29), 8219–8240. <https://doi.org/10.1039/C002653K>.

- (16) DiStasio, R. A.; von Helden, G.; Steele, R. P.; Head-Gordon, M. On the T-Shaped Structures of the Benzene Dimer. *Chem. Phys. Lett.* **2007**, *437* (4), 277–283. <https://doi.org/10.1016/j.cplett.2007.02.034>.
- (17) Podeszwa, R.; Bukowski, R.; Szalewicz, K. Potential Energy Surface for the Benzene Dimer and Perturbational Analysis of  $\Pi$ - $\pi$  Interactions. *J. Phys. Chem. A* **2006**, *110* (34), 10345–10354. <https://doi.org/10.1021/jp064095o>.
- (18) Pitoňák, M.; Neogrády, P.; Řezáč, J.; Jurečka, P.; Urban, M.; Hobza, P. Benzene Dimer: High-Level Wave Function and Density Functional Theory Calculations. *J. Chem. Theory Comput.* **2008**, *4* (11), 1829–1834. <https://doi.org/10.1021/ct800229h>.
- (19) Kumar Tummanapelli, A.; Vasudevan, S. Communication: Benzene Dimer—The Free Energy Landscape. *J. Chem. Phys.* **2013**, *139* (20), 201102. <https://doi.org/10.1063/1.4834855>.
- (20) Grant Hill, J.; Platts, J. A.; Werner, H.-J. Calculation of Intermolecular Interactions in the Benzene Dimer Using Coupled-Cluster and Local Electron Correlation Methods. *Phys. Chem. Chem. Phys.* **2006**, *8* (35), 4072. <https://doi.org/10.1039/b608623c>.
- (21) Azadi, S.; Cohen, R. E. Chemical Accuracy from Quantum Monte Carlo for the Benzene Dimer. *J. Chem. Phys.* **2015**, *143* (10), 104301. <https://doi.org/10.1063/1.4930137>.
- (22) Tsuzuki, S.; Uchimaru, T.; Sugawara, K.; Mikami, M. Energy Profile of the Interconversion Path between T-Shape and Slipped-Parallel Benzene Dimers. *J. Chem. Phys.* **2002**, *117* (24), 11216–11221. <https://doi.org/10.1063/1.1523057>.
- (23) Jaffe, R. L.; Smith, G. D. A Quantum Chemistry Study of Benzene Dimer. *J. Chem. Phys.* **1996**, *105* (7), 2780–2788. <https://doi.org/10.1063/1.472140>.
- (24) Lee, E. C.; Kim, D.; Jurečka, P.; Tarakeshwar, P.; Hobza, P.; Kim, K. S. Understanding of Assembly Phenomena by Aromatic–Aromatic Interactions: Benzene Dimer and the Substituted Systems. *J. Phys. Chem. A* **2007**, *111* (18), 3446–3457. <https://doi.org/10.1021/jp068635t>.
- (25) Sherrill, C. D.; Takatani, T.; Hohenstein, E. G. An Assessment of Theoretical Methods for Nonbonded Interactions: Comparison to Complete Basis Set Limit Coupled-Cluster Potential Energy Curves for the Benzene Dimer, the Methane Dimer, Benzene–Methane, and Benzene–H<sub>2</sub>S. *J. Phys. Chem. A* **2009**, *113* (38), 10146–10159. <https://doi.org/10.1021/jp9034375>.
- (26) Karton, A.; Martin, J. M. L. Prototypical  $\pi$ - $\pi$  Dimers Re-Examined by Means of High-Level CCSDT(Q) Composite Ab Initio Methods. *J. Chem. Phys.* **2021**, *154* (12), 124117. <https://doi.org/10.1063/5.0043046>.
- (27) Schnell, M.; Erlekam, U.; Bunker, P.; Helden, G. von; Grabow, J.-U.; Meijer, G.; Avoird, A. van der. Unraveling the Internal Dynamics of the Benzene Dimer: A Combined Theoretical and Microwave Spectroscopy Study. *Phys. Chem. Chem. Phys.* **2013**, *15* (25), 10207–10223. <https://doi.org/10.1039/C3CP51181B>.
- (28) Heindel, J. P.; Xantheas, S. S. The Many-Body Expansion for Aqueous Systems Revisited: I. Water–Water Interactions. *J. Chem. Theory Comput.* **2020**, *16* (11), 6843–6855. <https://doi.org/10.1021/acs.jctc.9b00749>.
- (29) Perdew, J. P.; Schmidt, K. *Density Functional Theory and Its Application to Materials: Antwerp, Belgium, 8-10 June 2000*; Van Doren, V. E., Van Alsenoy, C., Geerlings, P., Eds.; AIP conference proceedings; American Institute of Physics: Melville, N.Y., 2001.
- (30) Perdew, J. P.; Ruzsinszky, A.; Tao, J.; Staroverov, V. N.; Scuseria, G. E.; Csonka, G. I. Prescription for the Design and Selection of Density Functional Approximations: More

- Constraint Satisfaction with Fewer Fits. *J. Chem. Phys.* **2005**, *123* (6), 062201. <https://doi.org/10.1063/1.1904565>.
- (31) Mardirossian, N.; Lambrecht, D. S.; McCaslin, L.; Xantheas, S. S.; Head-Gordon, M. The Performance of Density Functionals for Sulfate–Water Clusters. *J. Chem. Theory Comput.* **2013**, *9* (3), 1368–1380. <https://doi.org/10.1021/ct4000235>.
- (32) Goerigk, L.; Hansen, A.; Bauer, C.; Ehrlich, S.; Najibi, A.; Grimme, S. A Look at the Density Functional Theory Zoo with the Advanced GMTKN55 Database for General Main Group Thermochemistry, Kinetics and Noncovalent Interactions. *Phys. Chem. Chem. Phys.* **2017**, *19* (48), 32184–32215. <https://doi.org/10.1039/C7CP04913G>.
- (33) Grimme, S. Density Functional Theory with London Dispersion Corrections. *WIREs Comput. Mol. Sci.* **2011**, *1* (2), 211–228. <https://doi.org/10.1002/wcms.30>.
- (34) Grimme, S.; Antony, J.; Ehrlich, S.; Krieg, H. A Consistent and Accurate *Ab Initio* Parametrization of Density Functional Dispersion Correction (DFT-D) for the 94 Elements H–Pu. *J. Chem. Phys.* **2010**, *132* (15), 154104. <https://doi.org/10.1063/1.3382344>.
- (35) Dunning, T. H. Gaussian Basis Sets for Use in Correlated Molecular Calculations. I. The Atoms Boron through Neon and Hydrogen. *J. Chem. Phys.* **1989**, *90* (2), 1007–1023. <https://doi.org/10.1063/1.456153>.
- (36) Peterson, K. A.; Woon, D. E.; Dunning, Jr., T. H. Benchmark Calculations with Correlated Molecular Wave Functions. IV. The Classical Barrier Height of the  $\text{H}+\text{H}_2\rightarrow\text{H}_2+\text{H}$  Reaction. *J. Chem. Phys.* **1994**, *100* (10), 7410–7415. <https://doi.org/10.1063/1.466884>.
- (37) Woon, D. E.; Dunning, T. H. Benchmark Calculations with Correlated Molecular Wave Functions. I. Multireference Configuration Interaction Calculations for the Second Row Diatomic Hydrides. *J. Chem. Phys.* **1993**, *99* (3), 1914–1929. <https://doi.org/10.1063/1.465306>.
- (38) Peterson, K. A.; Kendall, R. A.; Dunning, T. H. Benchmark Calculations with Correlated Molecular Wave Functions. II. Configuration Interaction Calculations on First Row Diatomic Hydrides. *J. Chem. Phys.* **1993**, *99* (3), 1930–1944. <https://doi.org/10.1063/1.465307>.
- (39) Peterson, K. A.; Kendall, R. A.; Dunning, T. H. Benchmark Calculations with Correlated Molecular Wave Functions. III. Configuration Interaction Calculations on First Row Homonuclear Diatomics. *J. Chem. Phys.* **1993**, *99* (12), 9790–9805. <https://doi.org/10.1063/1.465461>.
- (40) Dunning, T. H. A Road Map for the Calculation of Molecular Binding Energies. *J. Phys. Chem. A* **2000**, *104* (40), 9062–9080. <https://doi.org/10.1021/jp001507z>.
- (41) Xantheas, S. S.; Burnham, C. J.; Harrison, R. J. Development of Transferable Interaction Models for Water. II. Accurate Energetics of the First Few Water Clusters from First Principles. *J. Chem. Phys.* **2002**, *116* (4), 1493–1499. <https://doi.org/10.1063/1.1423941>.
- (42) Miliordos, E.; Xantheas, S. S. An Accurate and Efficient Computational Protocol for Obtaining the Complete Basis Set Limits of the Binding Energies of Water Clusters at the MP2 and CCSD(T) Levels of Theory: Application to  $(\text{H}_2\text{O})_m$ ,  $m = 2-6, 8, 11, 16$ , and 17. *J. Chem. Phys.* **2015**, *142* (23), 234303. <https://doi.org/10.1063/1.4922262>.
- (43) Jung, Y.; Lochan, R. C.; Dutoi, A. D.; Head-Gordon, M. Scaled Opposite-Spin Second Order Møller–Plesset Correlation Energy: An Economical Electronic Structure Method. *J. Chem. Phys.* **2004**, *121* (20), 9793–9802. <https://doi.org/10.1063/1.1809602>.
- (44) Gerenkamp, M.; Grimme, S. Spin-Component Scaled Second-Order Møller–Plesset Perturbation Theory for the Calculation of Molecular Geometries and Harmonic

- Vibrational Frequencies. *Chem. Phys. Lett.* **2004**, *392* (1), 229–235.  
<https://doi.org/10.1016/j.cplett.2004.05.063>.
- (45) Distasio JR., R. A.; Head-Gordon, M. Optimized Spin-Component Scaled Second-Order Møller-Plesset Perturbation Theory for Intermolecular Interaction Energies. *Mol. Phys.* **2007**, *105* (8), 1073–1083. <https://doi.org/10.1080/00268970701283781>.
- (46) Boys, S. F.; Bernardi, F. The Calculation of Small Molecular Interactions by the Differences of Separate Total Energies. Some Procedures with Reduced Errors. *Mol. Phys.* **1970**, *19* (4), 553–566. <https://doi.org/10.1080/00268977000101561>.
- (47) Xantheas, S. S. On the Importance of the Fragment Relaxation Energy Terms in the Estimation of the Basis Set Superposition Error Correction to the Intermolecular Interaction Energy. *J. Chem. Phys.* **1996**, *104* (21), 8821–8824.  
<https://doi.org/10.1063/1.471605>.
- (48) Aprà, E.; Bylaska, E. J.; de Jong, W. A.; Govind, N.; Kowalski, K.; Straatsma, T. P.; Valiev, M.; van Dam, H. J. J.; Alexeev, Y.; Anchell, J.; Anisimov, V.; Aquino, F. W.; Atta-Fynn, R.; Autschbach, J.; Bauman, N. P.; Becca, J. C.; Bernholdt, D. E.; Bhaskaran-Nair, K.; Bogatko, S.; Borowski, P.; Boschen, J.; Brabec, J.; Bruner, A.; Cauët, E.; Chen, Y.; Chuev, G. N.; Cramer, C. J.; Daily, J.; Deegan, M. J. O.; Dunning, T. H.; Dupuis, M.; Dyall, K. G.; Fann, G. I.; Fischer, S. A.; Fonari, A.; Früchtl, H.; Gagliardi, L.; Garza, J.; Gawande, N.; Ghosh, S.; Glaesemann, K.; Götz, A. W.; Hammond, J.; Helms, V.; Hermes, E. D.; Hirao, K.; Hirata, S.; Jacquelin, M.; Jensen, L.; Johnson, B. G.; Jónsson, H.; Kendall, R. A.; Klemm, M.; Kobayashi, R.; Konkov, V.; Krishnamoorthy, S.; Krishnan, M.; Lin, Z.; Lins, R. D.; Littlefield, R. J.; Logsdail, A. J.; Lopata, K.; Ma, W.; Marenich, A. V.; Martin del Campo, J.; Mejia-Rodriguez, D.; Moore, J. E.; Mullin, J. M.; Nakajima, T.; Nascimento, D. R.; Nichols, J. A.; Nichols, P. J.; Nieplocha, J.; Otero-de-la-Roza, A.; Palmer, B.; Panyala, A.; Pirojsirikul, T.; Peng, B.; Peverati, R.; Pittner, J.; Pollack, L.; Richard, R. M.; Sadayappan, P.; Schatz, G. C.; Shelton, W. A.; Silverstein, D. W.; Smith, D. M. A.; Soares, T. A.; Song, D.; Swart, M.; Taylor, H. L.; Thomas, G. S.; Tipparaju, V.; Truhlar, D. G.; Tsemekhman, K.; Van Voorhis, T.; Vázquez-Mayagoitia, Á.; Verma, P.; Villa, O.; Vishnu, A.; Vogiatzis, K. D.; Wang, D.; Weare, J. H.; Williamson, M. J.; Windus, T. L.; Woliński, K.; Wong, A. T.; Wu, Q.; Yang, C.; Yu, Q.; Zacharias, M.; Zhang, Z.; Zhao, Y.; Harrison, R. J. NWChem: Past, Present, and Future. *J. Chem. Phys.* **2020**, *152* (18), 184102. <https://doi.org/10.1063/5.0004997>.
- (49) Hohenberg, P.; Kohn, W. Inhomogeneous Electron Gas. *Phys. Rev.* **1964**, *136* (3B), B864–B871. <https://doi.org/10.1103/PhysRev.136.B864>.
- (50) Kohn, W.; Sham, L. J. Self-Consistent Equations Including Exchange and Correlation Effects. *Phys. Rev.* **1965**, *140* (4A), A1133–A1138.  
<https://doi.org/10.1103/PhysRev.140.A1133>.
- (51) Slater, J. C. Quantum Theory of Molecules and Solids Vol. 4: The Self-Consistent Field for Molecules and Solids. *Phys. Today* **1974**, *27* (12), 49–50.  
<https://doi.org/10.1063/1.3129035>.
- (52) Vosko, S. H.; Wilk, L.; Nusair, M. Accurate Spin-Dependent Electron Liquid Correlation Energies for Local Spin Density Calculations: A Critical Analysis. *Can. J. Phys.* **1980**, *58* (8), 1200–1211. <https://doi.org/10.1139/p80-159>.
- (53) Slater, J. C.; Johnson, K. H. Self-Consistent-Field X $\alpha$  Cluster Method for Polyatomic Molecules and Solids. *Phys. Rev. B* **1972**, *5* (3), 844–853.  
<https://doi.org/10.1103/PhysRevB.5.844>.

- (54) Perdew, J. P.; Burke, K.; Ernzerhof, M. Generalized Gradient Approximation Made Simple. *Phys. Rev. Lett.* **1996**, *77* (18), 3865–3868. <https://doi.org/10.1103/PhysRevLett.77.3865>.
- (55) Tao, J.; Perdew, J. P.; Staroverov, V. N.; Scuseria, G. E. Climbing the Density Functional Ladder: Nonempirical Meta-Generalized Gradient Approximation Designed for Molecules and Solids. *Phys. Rev. Lett.* **2003**, *91* (14), 146401. <https://doi.org/10.1103/PhysRevLett.91.146401>.
- (56) Zhao, Y.; Truhlar, D. G. A New Local Density Functional for Main-Group Thermochemistry, Transition Metal Bonding, Thermochemical Kinetics, and Noncovalent Interactions. *J. Chem. Phys.* **2006**, *125* (19), 194101. <https://doi.org/10.1063/1.2370993>.
- (57) Peverati, R.; Truhlar, D. G. M11-L: A Local Density Functional That Provides Improved Accuracy for Electronic Structure Calculations in Chemistry and Physics. *J. Phys. Chem. Lett.* **2012**, *3* (1), 117–124. <https://doi.org/10.1021/jz201525m>.
- (58) Peverati, R.; Truhlar, D. G. Improving the Accuracy of Hybrid Meta-GGA Density Functionals by Range Separation. *J. Phys. Chem. Lett.* **2011**, *2* (21), 2810–2817. <https://doi.org/10.1021/jz201170d>.
- (59) Zhao, Y.; Truhlar, D. G. The M06 Suite of Density Functionals for Main Group Thermochemistry, Thermochemical Kinetics, Noncovalent Interactions, Excited States, and Transition Elements: Two New Functionals and Systematic Testing of Four M06-Class Functionals and 12 Other Functionals. *Theor. Chem. Acc.* **2008**, *120* (1), 215–241. <https://doi.org/10.1007/s00214-007-0310-x>.
- (60) Becke, A. D. Density-functional Thermochemistry. III. The Role of Exact Exchange. *J. Chem. Phys.* **1993**, *98* (7), 5648–5652. <https://doi.org/10.1063/1.464913>.
- (61) Stephens, P. J.; Devlin, F. J.; Chabalowski, C. F.; Frisch, M. J. Ab Initio Calculation of Vibrational Absorption and Circular Dichroism Spectra Using Density Functional Force Fields. *J. Phys. Chem.* **1994**, *98* (45), 11623–11627. <https://doi.org/10.1021/j100096a001>.
- (62) Adamo, C.; Barone, V. Toward Reliable Density Functional Methods without Adjustable Parameters: The PBE0 Model. *J. Chem. Phys.* **1999**, *110* (13), 6158–6170. <https://doi.org/10.1063/1.478522>.
- (63) Chai, J.-D.; Head-Gordon, M. Long-Range Corrected Hybrid Density Functionals with Damped Atom–Atom Dispersion Corrections. *Phys. Chem. Chem. Phys.* **2008**, *10* (44), 6615–6620. <https://doi.org/10.1039/B810189B>.
- (64) Grimme, S. Semiempirical GGA-type density functional constructed with a long-range dispersion correction. *J. Comput. Chem.* **2006**, *27* (15), 1787–1799. <https://doi.org/10.1002/jcc.20495>.
- (65) Schmider, H. L.; Becke, A. D. Optimized Density Functionals from the Extended G2 Test Set. *J. Chem. Phys.* **1998**, *108* (23), 9624–9631. <https://doi.org/10.1063/1.476438>.
- (66) Grimme, S. Semiempirical Hybrid Density Functional with Perturbative Second-Order Correlation. *J. Chem. Phys.* **2006**, *124* (3), 034108. <https://doi.org/10.1063/1.2148954>.
- (67) M. J. Frisch, G. W. Trucks, H. B. Schlegel, G. E. Scuseria, M. A. Robb, J. R. Cheeseman, G. Scalmani, V. Barone, G. A. Petersson, H. Nakatsuji, X. Li, M. Caricato, A. Marenich, J. Bloino, B. G. Janesko, R. Gomperts, B. Mennucci, H. P. Hratchian, J. V. Ortiz, A. F. Izmaylov, J. L. Sonnenberg, D. Williams-Young, F. Ding, F. Lipparini, F. Egidi, J. Goings, B. Peng, A. Petrone, T. Henderson, D. Ranasinghe, V. G. Zakrzewski, J. Gao, N. Rega, G. Zheng, W. Liang, M. Hada, M. Ehara, K. Toyota, R. Fukuda, J. Hasegawa, M. Ishida, T. Nakajima, Y. Honda, O. Kitao, H. Nakai, T. Vreven, K. Throssell, J. A.

- Montgomery, Jr., J. E. Peralta, F. Ogliaro, M. Bearpark, J. J. Heyd, E. Brothers, K. N. Kudin, V. N. Staroverov, T. Keith, R. Kobayashi, J. Normand, K. Raghavachari, A. Rendell, J. C. Burant, S. S. Iyengar, J. Tomasi, M. Cossi, J. M. Millam, M. Klene, C. Adamo, R. Cammi, J. W. Ochterski, R. L. Martin, K. Morokuma, O. Farkas, J. B. Foresman, and D. J. Fox. Gaussian 09, Revision E.01, 2013.
- (68) Sinnokrot, M. O.; Sherrill, C. D. Highly Accurate Coupled Cluster Potential Energy Curves for the Benzene Dimer: Sandwich, T-Shaped, and Parallel-Displaced Configurations. *J. Phys. Chem. A* **2004**, *108* (46), 10200–10207.  
<https://doi.org/10.1021/jp0469517>.
- (69) Arunan, E.; Gutowsky, H. S. The Rotational Spectrum, Structure and Dynamics of a Benzene Dimer. *J. Chem. Phys.* **1993**, *98* (5), 4294–4296.  
<https://doi.org/10.1063/1.465035>.